Design of a temperature-controlled breast phantom for investigations into the temperature stability of a photoacoustic tomographic breast imager

A.J. Tijburg

BSc-Thesis Biomedical Technology
19 July 2022

Multi Modality Medical Imaging group
Faculty of Science and Technology
University of Twente

Examination committee

Daily supervisor: R.F.G. Bulthuis, MSc
External committee member: D. Thompson, MSc
Chair: prof. dr. S. Manohar

Multi-Modality M3i Medical Imaging
UNIVERSITY OF TWENTE.

Summary

Photoacoustic (PA) tomographic imaging is a promising technique to evaluate the response of breast cancer to neoadjuvant chemotherapy treatment. To bring this closer to regular application in clinical practice, high repeatability of image results is required. The objective of this study is to design and develop a temperature-controlled breast phantom that is suitable as a test object for investigations into the temperature fluctuations in the water in the imaging bowl of the PAMMOTH photoacoustic tomographic breast imager.

Based on considerations regarding the temperature stability of the test object, needed for repeated measurements, and the suitability for being used in a PA tomographic breast imaging system, a set of twelve requirements was made. Fabrication of the prototype and final design included vacuum shaping techniques and 3D printing. Characterization of the temperature stability and homogeneity of the phantom was done using thermocouples and an infrared camera. The test object was subsequently used in the PAMMOTH system to obtain PA reconstructions of the created temperature-controlled breast phantom.

The developed phantom consists of two main parts: a breast tissue-mimicking part and a temperature regulating system. The temperature system, being the innovative part of the phantom, consists of a heated water flow circuit that encapsulates the tissue-mimicking part. The encapsulating part of the flow circuit is composed of two vertically stacked, breast-shaped PVC cups, separated by a water supply ring. The ring is connected to a closed-loop pumping system that includes a water reservoir that is heated by a hot plate. The tissue-mimicking part was placed inside the inner PVC cup and consists of gel wax in which subresolution PA targets are embedded.

The encapsulating flowing water layer was shown to have a homogeneous temperature distribution, which remained stable over the duration of a PAMMOTH measurement. However, due to the shortcomings of the hot plate, there was limited control over the exact temperature at which it stabilized. The temperature of the gel wax was shown to cool down but at a very slow rate such that it could be considered stable over the duration of a PAMMOTH measurement. This conclusion applied only if the gel wax was homogeneously pre-heated to the same temperature as the water flowing through the water layer. Spatial temperature inhomogeneity in the gel wax will result in spatial inhomogeneity in the speed of sound inside the phantom, which may complicate the use of the phantom as a test object for PA reconstruction.

These findings imply that the developed phantom in its current state is not yet ready to be used as a test object in a repeatability study, as the temperature of the test object cannot be ensured to have exactly the same temperature in each repeated measurement. However, it is expected that improvements of the heating source for heating the water and better insulation of the gel wax on the top side of the phantom can improve the temperature stability of the phantom, thereby making it suitable for repeated measurements.

Contents

1 Introduction **6**

1.1 Clinical problem . . . 6

1.2 Research motivation . . . 7

1.3 Objective and research questions . . . 8

1.4 Thesis outine . . . 8

2 Background theory **10**

2.1 Breast cancer . . . 10

2.2 Photoacoustic imaging . . . 10

2.3 PAMMOTH breast imager . . . 12

2.4 Influence of temperature fluctuations in water . . . 12

3 Phantom requirements **15**

4 Concept designs and material choices **18**

4.1 Scoring system . . . 18

4.2 Phantom flow system concept designs . . . 19

4.3 Possible materials temperature system . . . 22

4.3.1 Temperature regulation . . . 22

4.3.2 Temperature monitoring . . . 22

4.4 Possible materials tissue-mimicking part . . . 23

4.4.1 Matrix material . . . 23

4.4.2 Photoacoustic targets . . . 25

5 Fabrication and characterization: Prototype phantom **27**

5.1 Prototype design . . . 27

5.2 Prototype fabrication . . . 30

5.2.1 Materials and methods . . . 30

5.2.2 Fabrication results . . . 31

5.3 Prototype characterization . . . 33
5.3.1 Materials and methods . . . 33
5.3.2 Characterization results . . . 34
5.4 Discussion and conclusion . . . 35

6 Fabrication and characterization: Final phantom 37
6.1 Final phantom design . . . 37
6.2 Final phantom fabrication . . . 38
6.2.1 Materials and methods . . . 38
6.2.2 Fabrication results . . . 39
6.3 Final phantom characterization . . . 40
6.3.1 Materials and methods . . . 41
6.3.2 Characterization results . . . 44
6.4 Discussion and conclusion . . . 48

7 Photoacoustic reconstructions 50
7.1 PAMMOTH measurements . . . 50
7.1.1 Materials and methods . . . 50
7.1.2 Results . . . 52
7.2 Discussion and conclusion . . . 54

8 Discussion 56

9 Conclusion 59
References . . . 61
References . . . 61

Appendices 64

A Cup mould and vacuum shaping PVC cups 65
A.1 ABS cup mould . . . 65
A.2 Protocol 1: Vacuum shaping PVC cups . . . 66

B Protocol 2: Coating microspheres with India ink 67

C Protocol 3: Gel wax casting 69

D Additional Characterization results 74
D.1 Gel wax pre-heating procedure . . . 74

E Thermocouple calibration 76

F Additional results temperature homogeneity **78**

G Additional results PA reconstructions **81**

List of acronyms

FWHM	Full width half maximum
MRI	Magnetic resonance imaging
MMG	Mammography
NIR	Near infrared
NAC	Neoadjuvant chemotherapy
PA	Photoacoustic
PSF	Point spread function
SOS	Speed of sound
ROF	Time of flight
US	Ultrasound

1 Introduction

1.1 Clinical problem

In 2020, female breast cancer accounted for 11.7 % of all cancer cases worldwide and as such became the most commonly diagnosed cancer type [1, 2]. Although the mortality rate of female breast cancer is declining since 1975 [3], breast cancer still accounted for 6.9% of all cancer deaths in 2020 [1]. The better survival outcomes over the years can be attributed to several possible factors, such as accurate early detection (e.g. mammographic screening) [ref Q] and improved adjuvant (post-operative) therapy [3, 4], which includes chemotherapy, radiation therapy, hormone therapy, targeted therapy, and biological therapy [5]. Also, Neoadjuvant chemotherapy (NAC), systemic therapy given before surgery, has contributed to improved cancer outcomes. Response rates to NAC are highest in patients with triple-negative and HER2-positive breast cancer subtypes [6]. NAC has shown to effectively downsize the tumor, even up to complete response (eradication of the tumor) in exceptional responders [7]. Lin *et al.* [7] have shown that NAC results in a noticeable decrease in tumor-associated angiogenesis [8], see Figure 1.1.

Current methods to assess cancer's response to NAC are x-ray mammography (MMG), ultrasonography, and magnetic resonance imaging (MRI) [7]. However, each technique has several drawbacks. MMG uses ionizing radiation, has a low detection sensitivity in dense breasts, and is often experienced as painful due to compression of the breast. Ultrasound has a relatively small field of view, is operator dependent, and has poor discrimination in solid tumors. MRI requires contrast agents to visualize the blood vessels, has low specificity, and is expensive and therefore not accessible to all. Because of these limitations, currently, the response to NAC treatment can be evaluated only after surgery [7]. Therefore, there is a need for a reliable noninvasive imaging modality to assess the response to NAC at several points in time.

An imaging technique that might have the potential for the assessment of responses to NAC is photoacoustic (PA) imaging [9, 10], which is a non-invasive imaging modality that combines advantages of optical and acoustic imaging. PA imaging shows high contrast arising from wavelength-specific optical absorption by biological chromophores, such as hemoglobin and deoxyhemoglobin. With PA imaging, it was shown that it is possible to visualize the blood vessels in the breast in 3D. This makes PA a potentially good technique to visualize the response to NAC by visualizing the change in tumor-associated angiogenesis.

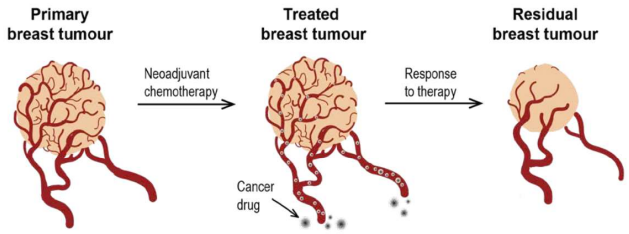

Figure 1.1: Schematic drawing of the effect of neoadjuvant chemotherapy on the vascularity of a tumor. Image made by Rianne F.G. Bulthuis.

1.2 Research motivation

The PAMMOTH [11] is a hybrid multispectral photoacoustic-ultrasound tomography system that can be used for breast imaging. One wants to investigate if the PAMMOTH imager is suitable to visualize the response to NAC over a period of time. For the PAMMOTH to be suitable, a highly stable performance is required. A stable performance means that photoacoustic (PA) reconstructions of repeated measurements are identical when a stable object is measured. In a system that is not highly stable, hardware instabilities may cause small changes in the PA reconstructions independent of actual changes in breast tissue, which leads possibly to misinterpretation of the images.

One of the instabilities of the PAMMOTH system is thought to be the temperature instability of the water in the imaging bowl that serves as a coupling medium between the breast and the ultrasound detectors. The temperature instabilities arise when the breast, which has a skin temperature ranging between 33-37 °C [12], contacts the 25 °C water in the imaging bowl. During patient measurements with the PAMMOTH system, temporal and spatial fluctuations in the water temperature were observed [R. Bulthuis, PhD thesis in progress]. Water temperature could change over time (during the measurement) when the water warms up when it contacts the body temperature breast and the temperature control system does not directly correct for this. Temperature fluctuations of approximately 1.5 - 2 °C were observed during patient measurements of 5 minutes. Besides, the water temperature is expected to have a spatial gradient. This might be due to water warming warm up around the surface of the breast and gradually spreading to the surrounding water via convection. Additionally, it could be from the electronics behind the imaging tank which generate heat. This results in a spatial gradient in the water in the opposite direction. Moreover, temperature fluctuation in the water could arise from internal fluctuations in the set temperature (25 °C) of the water, due to a slow feedback loop in the temperature control system.

In the PAMMOTH system, spatial distributions of the SOS in the breast can be obtained with US transmission measurements, as will be explained in section 2.3. These SOS distributions are based on an additional reference data set from SOS measurements with only water of 25 °C in the imaging bowl [11]. Consequently, temperature fluctuations and therefore SOS fluctuations in the water during patient measurements are currently not taken into account in the SOS map. This could affect the PA images since the SOS maps are used to reconstruct the PA images. Deviations in SOS can lead to displacement of absorbing structures in the reconstruction. Therefore, it is expected that reconstruction artifacts due to temperature fluctuations in the water appear as a blurring [13] and hence affect the resolution and contrast of the PA images.

A study of Van de Sompel *et al* (2012) [13] showed that a temperature decrease in the water of 1.5 °C (SOS change of 0.2%) can lead to image artifacts in photoacoustic tomography scans. The used photoacoustic system was the Nexus 128 scanner from Endra Life Sciences [REF]. They demonstrated the importance of continuously

monitoring the water temperature variations by applying software corrections for the corresponding variations in the speed of sound in the image reconstruction algorithm. This emphasizes the importance of the investigation of the effect of temperature instabilities in the water of the PAMMOTH system on the PA reconstructions.

1.3 Objective and research questions

Currently, it is unknown how large the effect of water temperature fluctuations is on the reconstructed PA images and whether this effect influences the stability of the performance of the PAMMOTH system. To investigate this, a repeatability study needs to be done with a highly stable test object (phantom) with a known composition and a controlled temperature. The objective of this study, therefore, is to design and develop a temperature-controlled phantom that is suitable for the investigation into the temperature fluctuations in the water of the imaging bowl.

This results in the following main research question:
How can a phantom be developed that is suitable for a repeatability study about the influence of water temperature fluctuations in the PAMMOTH on photoacoustic reconstructions?

In order to find an answer to the main research question, the following sub-questions are formulated:

- What are the requirements for the phantom to be suitable for investigation into water temperature fluctuations in the PAMMOTH?
- How stable and homogeneous is the temperature of the developed phantom?
- To what extent is the phantom suitable to be used for a repeatability study into the effect of water temperature fluctuations in the PAMMOTH?

1.4 Thesis outine

- **Chapter 2** provides background information on breast cancer, photoacoustic imaging, and the PAMMOTH imager. Also, the extent of the influence of speed of sound changes in water in the PAMMOTH imaging bowl is explained and supported with a calculation.
- **Chapter 3** explains the requirements for the phantom that will be developed.
- **Chapter 4** presents the first concept designs of the phantom, and several material choices for the phantom are made based on a scoring system and a SWOT-analysis (strengths, weaknesses, opportunities, and threats).
- **Chapter 5** starts with describing the prototype design. Subsequently, the fabrication and characterization of the prototype phantom are described. The results are discussed and based on that, several modifications are proposed to implement in the final phantom.
- **Chapter 6** describes the design, fabrication, and characterization of the final phantom, and the results are discussed.
- **Chapter 7** gives a demonstration of the final phantom in the PAMMOTH imager. Photoacoustic reconstructions will be shown and discussed.

- **Chapter 8** describes the overall discussion points of this study. It will be discussed to what extent the requirements were met, and how the phantom and the characterization experiments can be improved. Finally, recommendations are made for improvements to the phantom design and characterization.
- **Chapter 9** gives an overall conclusion about the suitability of the developed phantom for a repeatability study about the effect of water temperature fluctuations in the PAMMOTH on photoacoustic reconstructions.

Background theory

2

2.1 Breast cancer

Breast cancer refers to abnormally excessive proliferation of cells in breast tissues [14]. There are several types of breast cancers that can be classified into two major groups according to the origin of the affected cells, namely carcinomas and sarcomas [15]. Carcinomas are the most common type and arise from endothelial cells lining ducts and lobules in the glandular tissue of the breast. Sarcomas arise from stromal (supporting) tissues in the breast, which include fat and fibrous connective tissue. The invasiveness of the breast cancer type can be divided into three categories: non-invasive (in situ), invasive, and metastatic. Non-invasive breast cancer is confined to the location in the breast where the abnormal cells were found in the first place. When breast cancer is invasive it spreads to tissues surrounding the original tissue where the cancer cells developed. When breast cancer is metastatic, the tumor cells spread via blood or lymph to other organs in the body.

2.2 Photoacoustic imaging

Photoacoustic (optoacoustic) imaging [9, 10] is a non-invasive and hybrid medical imaging technique that combines optical excitation and acoustic detection. Advantages of PA imaging are the high contrast arising from specific optical absorption of excitation light, and high spatial resolution and deep penetration depth arising from the US. Photoacoustic (PA) imaging provides better resolution than optical imaging for depths greater than 1 mm since ultrasound scattering in biological tissues is 2-3 orders of magnitude weaker than optical scattering [16]. Other advantages are the use of non-ionizing laser radiation, endogenous tissue contrast, and speckle-free images.

PA imaging relies on the photoacoustic effect, which describes the generation of acoustic waves as a result of illumination of an absorbing substance with high energy, short-pulsed electromagnetic radiation [17]. The mechanism of photoacoustic signal generation is step-wise described in Figure 2.1. The excitation is typically achieved by illuminating tissue with nanosecond pulsed laser light in the near-infrared (NIR) spectrum [10] (2.1 step 1). The NIR wavelengths are used because optical absorption by biological soft tissues is relatively low in this range of the spectrum, thus allowing light to penetrate deeper into tissue [18]. The excitation light propagates through the tissue, undergoing scattering, and gets selectively (wavelength dependent) absorbed by chromophores in the tissue such as melanin in the skin or hemoglobin and oxyhemoglobin in the blood [19]. Absorption of the optical energy causes local a temperature rise which results in rapid thermoelastic expansion (2.1 step 2). This produces a pressure wave in the ultrasound (US) regime (2.1 step 3). The initial photoacoustic pressure (p_0) can be related to the light absorption via the Grüneisen parameter (Γ) by the following expression [17]

$$p_0(r) = \Gamma \mu_a F(r), \tag{2.1}$$

where μ_a is the absorption coefficient of the absorbing structure and F is the local optical fluence dependent on the travel distance r. The product of the absorption coefficient and the local optical fluences describes the absorbed energy density. The Grüneisen parameter can be expressed as

$$\Gamma = \frac{\beta c_s^2}{C_V}, \tag{2.2}$$

where β is the thermal expansion coefficient, C_V is the specific heat capacity at constant volume, and c_s is the speed of sound.

The generated pressure wave propagates through the tissue, with low scattering, and can be detected by multiple US transducers surrounding the tissue (2.1 step 4). By analyzing the detected US waves, an approximation of the initial pressure map can be reconstructed which gives an indication of the absorbed energy and hence provides information about the position, size and shape of the absorbing structure (2.1 step 5). In most PA reconstruction algorithms it is assumed that the tissue is homogeneous such that a single SOS value can be assigned to the entire tissue volume [20]. The distance of the absorber from the detectors can then be estimated by back-projection along circular paths, by multiplying the arrival time of the US wave at the detectors with the SOS in the tissue. This distance can be displayed as concentric circles, see figure 2.1. The location of the absorber is estimated to be at the intersection of the concentric circles.

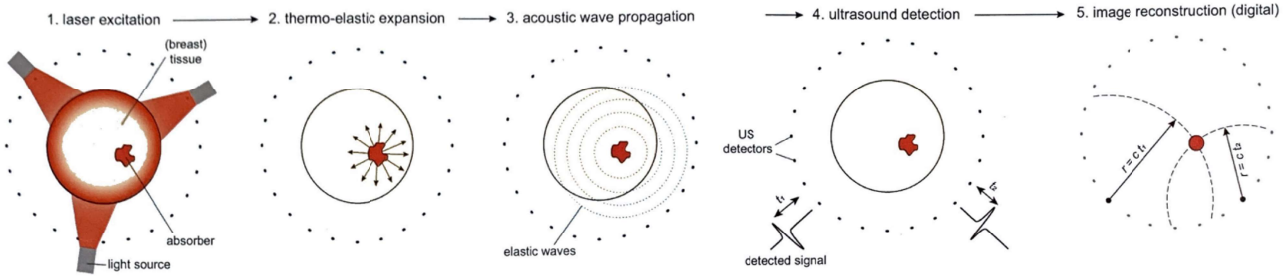

Figure 2.1: Schematic image of photoacoustic signal generation, propagation, and image formation. 1) Illumination of the tissue with short-pulsed laser light. 2) Absorbed energy induces thermoelastic expansion of the absorber. 3) As a result a pressure wave in the US regime is generated, which propagates through the tissue. 4) The ultrasound wave is detected by the transducers. 5) The distance from the absorber to the detector (r) is calculated by multiplying the measured time of arrival (t), with the speed of sound (c) in the tissue. Figure from Ref. [11].

A condition for the generation of a photoacoustic pressure wave is that the excitation is time-varying. If the pulse time of the laser is shorter than the thermal and stress confinement times, the conversion into acoustic signal is more efficient [17]. Pulse times shorter than the thermal confinement time indicate that the absorber is heated without thermal diffusion (no energy dissipation to the surrounding). Pulse times shorter than the stress confinement time indicate that there is no volume expansion of the absorbers during the illumination. Light pulses with pulse times in the nanosecond range satisfy both confinements.

The spatial resolution of a PA imaging system is a measure for the ability of the system to discern two closely-spaced absorbers from one another. A typical parameter to describe the spatial resolution of an imaging system is the full width half maximum (FWHM) of the point spread function (PSF) [20]. The PSF characterizes the response

of an imaging system to a point source. In an idealized imaging system, the PSF is a Dirac delta function, which will result in an exact reconstruction of the point source. In reality, the PSF is not a Dirac delta function because multiple (system) factors can lead to a degraded spatial resolution. These factors include characteristics of the ultrasound detectors (centre frequency, bandwidth, aperture size, and view angle), laser pulse duration, acoustic attenuation, and acoustic heterogeneity [20].

2.3 PAMMOTH breast imager

The PAMMOTH [11] is a hybrid multispectral photoacoustic-ultrasound tomography system that can be used for breast imaging, see Figure 2.2. The PAMMOTH imager is developed in a collaboration between the University of Twente and other European partners. The system consists of a 26 cm (inner diameter) hemispherical imaging bowl which contains 512 ultrasound (US) transducers with a centre frequency of 1 MHz (123 % bandwidth), and 40 optical fiber bundles coupled to a laser, see Figure 2.3. The imaging bowl is filled with 25 °C water which serves as an acoustic coupling medium between the breast and the US detectors. The water temperature is monitored by two PT100 temperature sensors at the bottom and the top of the bowl. A third temperature sensor is used in the feedback loop of the temperature control system in the PAMMOTH imager. The temperature of the water and the water level are regulated by a heating circulator (Dyneo DD 300F, Julabo, Seelbach, Germany). The fiber bundles illuminate the breast homogeneously with pulses with an excitation wavelength ranging from 680-1060 nm, a pulse duration of 4.2 ns, and a repetition rate of 10 Hz. The ultrasound transducers can send and receive ultrasound.

During a photoacoustic measurement, all transducers are in detection (receiving) mode and the imaging bowl rotates around its central axis such that multiple projections of the breast are made. During a measurement, the breast is immobilized in a transparent cup to reduce movement artifacts and to ensure a reproducible position of the breast in the center of the field-of-view [21]. Photoacoustic reconstructions are made using a full-wave inversion model. In photoacoustic reconstructions, the blood vessels could be visualized in 3D, because hemoglobin and deoxyhemoglobin in the blood can absorb the excitation light. In vivo, a resolution of 0.42 mm and an imaging depth of 48 mm was observed [11].

With the PAMMOTH system it is also possible to make speed of sound (SOS) maps. SOS maps are reconstructed from ultrasound transmission measurements in which one transducer element emits US and all other transducer elements detect. The SOS map provides information for breast cancer diagnosis, gives structural information, and a density characterization of breast tissue. Moreover, SOS maps are used to improve the quality of PA reconstructions, because it accounts for SOS differences of different tissues in the breast (e.g. fat and fibroglandular tissue). The SOS is calculated with a first arrival algorithm, using the time-of-flights (TOFs). This requires a reference data set that is obtained by a measurement with only water in the imaging bowl.

2.4 Influence of temperature fluctuations in water

It is known from literature that SOS in water depends on the temperature of the water. Del Grosso and Mader (1972) [22] described the speed of sound in water as a function of temperature with a fifth-order polynomial applicable over the range 0 - 100 °C:

$$c_s = \sum_{i=0}^{5} a_i T^i, \tag{2.3}$$

Figure 2.2: The PAMMOTH photoacoustic tomographic breast imager, positioned in the MST hospital in Oldenzaal.

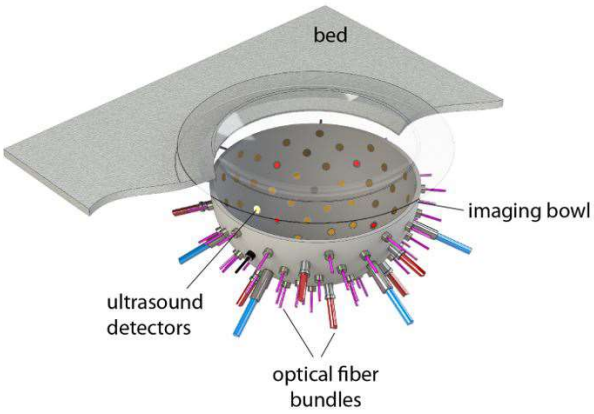

Figure 2.3: Schematic drawing of the PAMMOTH imaging bowl (diameter 26 cm), in which 512 US transducers and 40 optical fibre bundles are included. The imaging bowl is filled with 25 °C water that functions as acoustic coupling medium.

where c_s is the speed of sound (m/s), T is the water temperature (°C) and $a_0 - a_5$ are coefficients determined by a least-squares fit, resulting in a_0= 1402.388, $a_1 = 5.03711$, $a_2 = -5.80852 \cdot 10^{-2}$, $a_3 = 3.3420 \cdot 10^{-4}$, $a_4 = -1.4780 \cdot 10^{-6}$, and $a_5 = 3.146 \cdot 10^{-9}$. The resulting plot of speed of sound in water as a function of temperature is shown is Figure 2.4. The speed of sound at the set temperature of 25 °C is 1496.7 m/s. Temperature fluctuations of 1.5 °C above and below 25 °C will lead to a variation is speed of sound, ranging from 1492.6 m/s at 23.5 °C to 1500.6 m/s at 26.5 °C.

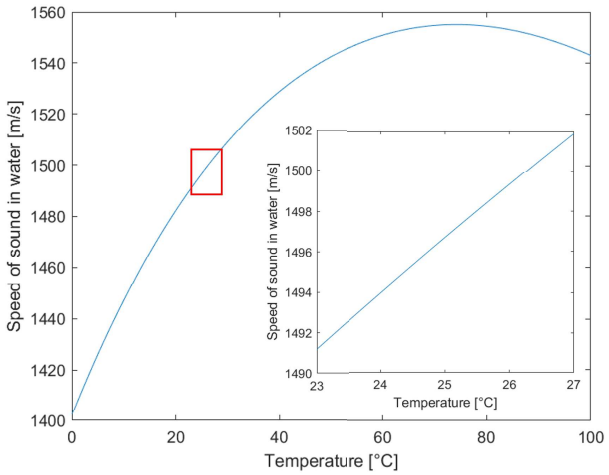

Figure 2.4: Speed of sound in water as a function of temperature, described by fifth-order polynomial and applicable over the range 0 - 100 °C. Insert graph shows the region of interest with water temperature fluctuations around 25 °C.

With a simplified calculation, it can be estimated how large the effect of a certain water temperature fluctuation is on the reconstructed PA image. The set temperature of the water is assumed to be 25 °C, which corresponds to a speed of sound (c_1) of 1496.7 m/s, see Figure 2.4. During patient measurements, water temperature fluctuations (ΔT) of approximately 1.5 °C were observed, which corresponds to a speed of sound (c_2) ranging from 1492.6 m/s at 23.5 °C to 1500.6 m/s at 26.5 °C. A deviation from the set temperature of the water will lead to a deviation

in the speed of sound, and this will lead to a different arrival time of a PA ultrasound wave at the detector. The difference in arrival time due to a fluctuation in water temperature can be calculated with:

$$\Delta t = \frac{d}{c_2} - \frac{d}{c_1} = \frac{d(c_1 - c_2)}{c_1 c_2}, \tag{2.4}$$

where Δt (in s) is the difference in arrival time of an US wave, d is the distance from the US transducer to the surface of the breast, c_1 is the speed of sound in water (in m/s) at the set temperature (25 °C), c_2 is the speed of sound in water after a temperature fluctuation of ΔT. For this calculation the water temperature fluctuation is assumed to be homogeneously distributed over the whole volume of water in the imaging bowl, so no spatial gradient is taken into account. The speed of sound changes in the water as result of temperature fluctuations can be calculated with Equation 2.3. Differences in arrival time due to SOS fluctuations lead to displacements in the PA images, because the SOS is used for the reconstructions, as explained in section 2.2. Equation 2.5 can be used to calculate the displacement (Δd) resulting from a certain temperature fluctuation.

$$\Delta d = c_1 \cdot \Delta t \tag{2.5}$$

In this Equation, c_1 is the speed of sound in water at the set temperature, and Δt can be calculated with Equation 2.4. In Figure 2.5, a graph of the displacement as a function of temperature fluctuation is shown. A temperature decrease of 1.5 °C (ΔT = -1.5 °C) will lead to a displacement of 192 μm. A temperature increase of 1.5 °C (ΔT = 1.5 °C) will lead to a displacement of -183 μm. In Figure 2.6 a schematic drawing of the breast in the imaging bowl is shown. A positive displacement refers to a displacement towards the centre of the bowl, while a negative displacement refers to a displacement away from the centre.

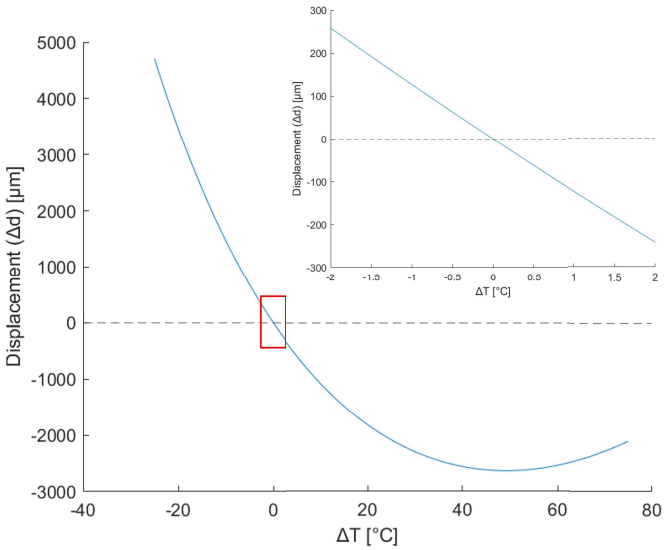

Figure 2.5: Graph of the displacement Δd caused by water temperature fluctuation ΔT, where 25 °C is taken as reference temperature and d is assumed to be 70 mm. Graph insert shows the region of interest with ΔT of ± 2 °C.

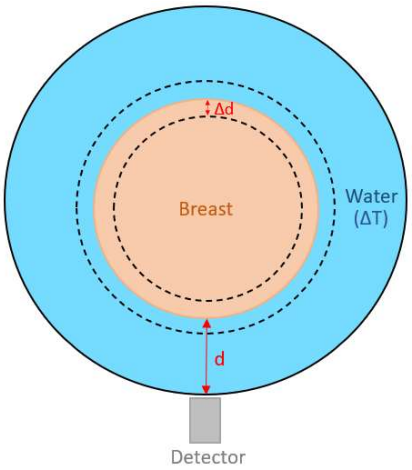

Figure 2.6: Schematic drawing of the breast in the imaging bowl, with d the distance from the transducer to the breast surface and Δd the displacement caused by water temperature fluctuation ΔT.

Phantom requirements

3

The objective is to design a temperature-controlled breast phantom that is suitable for investigation of the effect of temperature fluctuations of the water in the imaging bowl of the PAMMOTH. The phantom requirements are presented in Table 3.1 and will be discussed in more detail.

Requirement I: The phantom should have a realistic size, shape and volume such that it fits inside the imaging bowl of the PAMMOTH system, which has an inner diameter of 26 cm. Moreover, it ensures that the contact surface with the water in the imaging bowl is realistic and therefore likely heats a realistic volume of the water in the imaging bowl. Huang *et al* [23] reported ranges of breast diameter, breast length and breast volume, based on a breast CT data set of 216 women with bra cup sizes ranging from A until D, see Table 3.1.

Requirement II: temporal stability and re-usability is a highly important requirement since the phantom needs to be used for a repeatability study. If the phantom's material is not stable over a period of time, it will be unclear whether changes in PA images are due to instabilities in the PAMMOTH system or due to changes in the phantom itself.

Requirement III & IV: See description a,nd specification in Table 3.1

Requirement V: The material used should have a SOS value comparable to breast tissue because in repeatability studies the possible target displacements in the phantom should be relevant to displacements of absorbing structures (like blood vessels) in real breast tissue.

Requirement VI: Photoacoustic targets should be included in the phantom to generate a photoacoustic signal. The targets must absorb the excitation light, such that via the PA effect, a pressure wave is generated that can be detected. The reconstructed targets are necessary to investigate possible effects on the resolution.

Requirement VII: The targets must stay at a fixed position, such that PA reconstructions of repeated measurement could be compared to each other.

Requirement VIII: The used material should be stable in the range of body temperature ($\pm$ 37 °C), meaning that the melting temperature must be well above 37 °C. If the material starts to soften, this can lead to displacement of the PA targets. The mould in which the material will be casted must be resistant to higher temperatures because materials are often poured into the mould in a melted state. The exact required temperature is dependent on the

type of material.

Requirement IX: The phantom's material must be optically (semi) transparent, such that the excitation light of the laser can reach the PA targets. The material must also be acoustic (semi) transparent because the US waves generated by the PA targets (due to the PA effect) must be able to reach the detectors before being attenuated too much.

Requirement X: The phantom must have an adjustable temperature because various experiments must be conducted to investigate the effect of water temperature fluctuations. Measurements with the phantom at body temperature must be conducted. The skin temperature of the breast can range between 33-37 °C [12], and one or more of these temperatures could be chosen. Also reference measurements with a 25 °C phantom should be conducted, such that its temperature is similar to the temperature of the water in the imaging bowl, and in principle no temperature fluctuations are induced by the phantom.

Requirement XI: During a PAMMOTH measurement, it is important that the temperature of the phantom is as stable and homogeneous as possible. Fluctuations in temperatures result in fluctuations in SOS inside the phantom. If the SOS changes during a PA measurement, it is not possible to distinguish the effect of water temperature fluctuations from the effect of the temperature fluctuations inside the phantom itself. The phantom's temperature should remain stable for at least 5 minutes, because this is the typical time span for a PA measurement in the PAMMOTH. Also, a homogeneous temperature distribution is desired, because temperature gradients can drive instabilities.

Requirement XII: During a PAMMOTH measurement, it is important to accurately monitor the temperature inside the phantom. This provides 1) information about the stability of temperature (see requirement XI), and 2) absolute temperature values which are needed for photoacoustic reconstructions.

Table 3.1: Table of requirements for the photoacoustic breast phantom. The requirements have been scored on their importance with an importance factor (F) ranging from 1 (least important) to 5 (most important).

	Requirements	Descriptions/Specifications	Importance factor (F)
I	**Realistic size, shape and volume**	Breast diameter: 11.1-19.0 cm [23], Breast length: 5.7-9.2 cm Breast volume: 324.7 - 1203.7 ml	4
II	**Temporal stability and re-usable**	The phantom must remain stable for $>$ 6 months, and repeated use may not affect phantom stability	5
III	**Easy to fabricate**	Fabrication process must be reasonably easy and within short period of time ($<$ 1 week)	4
IV	**Mobile**	Phantom (incl. temperature system) must be transported to the hospital for PAMMOTH measurements	3
V	**Relevant range of acoustic properties**	SOS: 1430 - 1520 m/s [24] Acoustic attenuation: 1 - 25 dB/cm [24]	5 3
VI	**Photoacoustic targets** • Sub-resolution • Analyse image quality • Strongly absorb excitation light	 Target size $<$ 400 μm Determine resolution based on point spread functions Flat and perfect (100 %) absorbance at all excitation wavelengths, ideal (hyperblack) absorbers	5
VII	**Stability of target position**	Targets must stay at fixed positions inside the phantom	5
XIII	**Temperature resistant materials**	Materials must be stable at 37 °C, and moulds must resist higher temperatures	5
IX	**Use of materials that minimally affect photoacoustic signal**	Use of materials that are optically and acoustic (semi) transparent and avoid materials that generate a disturbing PA signal (e.g. metals)	4
X	**Adjustable temperature**	Temperature must be adjustable over a range of 20 - 40 °C	5
XI	**Stable and homogeneous temperature**	Phantom must remain constant at body temperature for at least 5 minutes	5
XII	**Temperature monitoring**	Temperature inside phantom should be known	4

4 Concept designs and material choices

In this chapter, several phantom concept designs are proposed. The focus of the concept designs will be a design for a temperature regulating system, as this is the innovative part of this phantom. Also, an overview of potentially useful materials for the phantom is given. Through a scoring system and a SWOT-analysis (strengths, weaknesses, opportunities, and threats), the most promising concept design and materials are selected.

4.1 Scoring system

The requirements have been scored on their importance with an importance factor (F) ranging from 1 to 5, where 1 denotes the least important requirement and 5 denotes the most important requirement. A SWOT-analysis is made for each concept design and the possible material choices. A SWOT-analysis describes the strengths, weaknesses, opportunities, and threats of each option. Each option gets a final score based on the SWOT-analysis, by taking into account the importance factor of the requirements. Strengths and weaknesses have a weight factor (W) of 1 and -1 respectively, while opportunities and threats have a weight factor of 0.5 and -0.5 respectively, see Table 4.1. This means that strengths and weaknesses are considered more important than opportunities and threats. In the SWOT-analysis the corresponding requirement is indicated inside parentheses. When an item in the SWOT-analysis does not match one of the established requirements, it will receive an importance factor of 1. The importance factor of a requirement will be multiplied by the corresponding weight factor of the SWOT-analysis. The final score is calculated by adding all weighted importance factors, as shown in Equation 4.1:

$$Finalscore = W_S \cdot (F_1 + F_2 + ...) + W_W \cdot (F_1 + F_2 + ...) + W_O \cdot (F_1 + F_2 + ...) + W_T \cdot (F_1 + F_2 + ...), \quad (4.1)$$

in which W_x is the weight factor (Table see 4.1) and F_x is the requirement importance factor in which x is the item number (1, 2, etc.) of the elements in the SWOT analysis.

Table 4.1: Weigth factors (W_x) for calculation of final scores for options in SWOT-analysis.

	Weight factor (W_x)
Strengths	1
Weaknesses	-1
Opportunities	0.5
Threats	-0.5

4.2 Phantom flow system concept designs

The goal is to design a breast phantom that maintains a stable body temperature during a PA measurement (typically 5 minutes) in the PAMMOTH system. This is because the phantom needs to be used to investigate the effect of water temperature fluctuations, which are induced when a warm breast contacts the 25 °C water in the imaging bowl. Based on the requirements in Chapter 3, three concept designs are created. All three concepts consist of two main parts: a tissue-mimicking part and a temperature regulating system. The tissue-mimicking part consists of a matrix material that ensures that the acoustic properties, especially speed of sound, are relevant to breast tissue. The temperature regulating system aims to mimic the body temperature of a real breast. It is minimally required to heat the surface of the phantom since this is the part that makes contact with the water in the imaging bowl. Although the core of the phantom does not necessarily need to be at body temperature, the temperature in the core should be very constant. The focus of the concept designs will be on the temperature regulating system, as this is the innovative part of this phantom. The design of the tissue-mimicking part is more well established in literature and therefore will not differ between the concepts.

The temperature regulating system will be based on a water flow circuit, heating the surface of the phantom that contacts the water in the imaging bowl. Water is chosen because it is already present in the imaging bowl as a coupling medium between the breast and the US transducers. The flow aims to create a stable temperature, by continuously refreshing with new warm water. The three designs differ in the way the inflow and outflow of the water are regulated and therefore differ in the way the water flows through the water circuit. This is relevant because the way the water flows could have an influence on the homogeneity of the surface temperature.

Design 1 is shown in Figure 4.1, and consists of an inner part of tissue-mimicking material (TMM) and a water flow circuit on the outer part of the phantom. The tissue-mimicking material consists of a matrix material in which PA targets are embedded. The water circuit covers the surface of the phantom which will be in contact with the water in the imaging bowl. Therefore, the top part of the phantom is not covered by the water circuit. Design 1 is the most simple design, in which there is only one water inflow and one outflow point. The water input and output points are placed on opposite sides to create a water flow through the outer layer of the phantom.

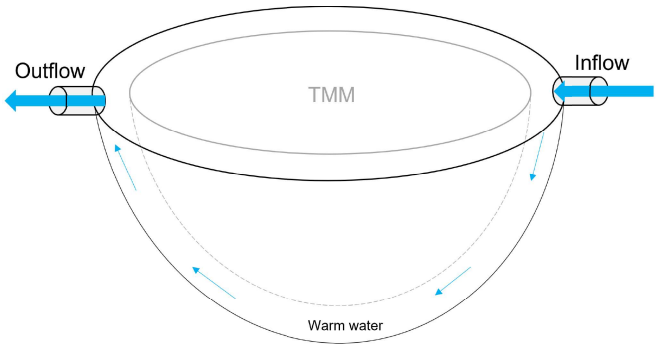

Figure 4.1: Schematic drawing of concept design 1. The design consist of an inner part of tissue-mimicking material (TMM) and a water flow circuit on the outer part of the phantom. In this design, there is only one point for water inflow and one for water outflow. The water input and output are placed on opposite sides to create a water flow through the outer layer.

Design 2 is shown in Figure 4.2, and consists of an inner part of tissue-mimicking material (TMM) and a water flow circuit on the outer part of the phantom, as explained in design 1. The water circuit consists of two separate

half rings on top part of the phantom. One half ring functions as a water input and the other as a water output. The ring contains several small holes along the circumference of the phantom to distribute the water input and output over the phantoms surface.The small holes in the ring aim to ensure a homogeneous water flow through the circuit.

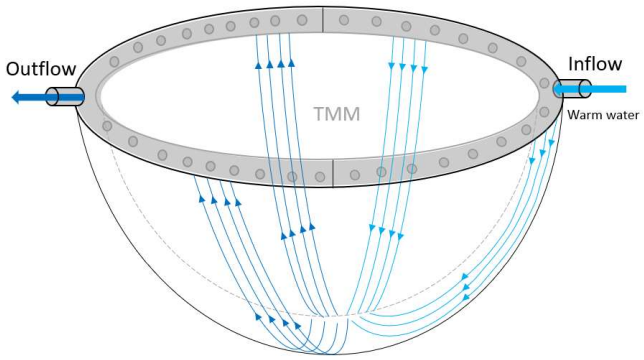

Figure 4.2: Schematic drawing of concept design 2. The design consist of an inner part of tissue-mimicking material (TMM) and a water flow circuit on the outer part of the phantom. In this design, the water inflow and outflow are divided into two separate half rings (in grey) with small holes in it. The right half ring is the water input and the left half ring is the water output. The light blue lines represent the water inflow and the dark blue lines the water outflow. Only a few lines are drawn to visualize the water flow along the ring.

Design 3 is shown in Figure 4.3, and consists of an inner part of tissue-mimicking ma rial (TMM) and a water flow circuit on the outer part of the phantom, as explained in design 1. The water flow circuit consists of one inflow tube and one outflow tube in the outer layer of the phantom. Each tube contains several holes, through which water can enter or exit the circuit. The holes are positioned on the left and on the right side of each tube to ensure the water equally flows along both sides of the phantom. The tube The tubes reach from the top to the bulge of the phantom and thereby aim to ensure homogeneous water flow around the entire surface of the phantom.

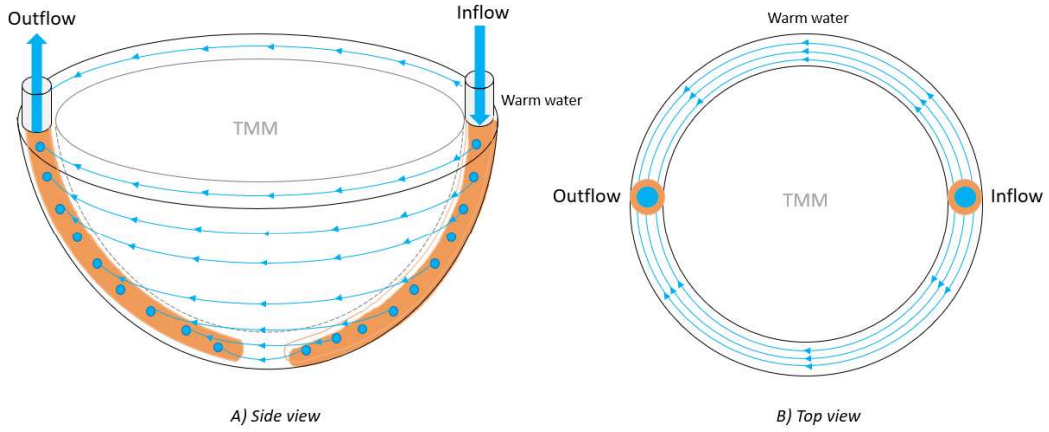

Figure 4.3: Schematic drawing of concept design 3, A) side view, and B) top view. The design consist of an inner part of tissue-mimicking material (TMM) and a water flow circuit on the outer part of the phantom. In this design, the water inflow and outflow are regulated via two tubes inside the surface of the phantom. The tubes contain holes on both sides to ensure homogeneous water flow around the entire surface of the phantom.

A SWOT-analysis is made for the different designs and is shown in Table 4.2.

Table 4.2: SWOT-analysis for the phantom concept design. Design 1-3 are shown in Figure 4.1 - 4.3. The characteristics of each design are categorised in strengths (S), weaknesses (W), opportunities (O) and threats (T). The corresponding requirement is indicated with a Roman numerals inside parentheses.

	Design 1	**Design 2**	**Design 3**
S	- Most simple design to fabricate (III) - No PA disturbing structures inside field of view (IX) - Water circuit allows a quickly adjustable surface temperature (X)	- More homogeneous water flow around surface of phantom (compared to design 1) (XI) - No PA disturbing structures inside field of view (IX) - Water circuit allows a quickly adjustable surface temperature (X)	- Homogeneous water (XI) flow around surface of phantom - Water circuit allows a quickly adjustable surface temperature (X)
W	- Likely no homogeneous water flow around surface of phantom, resulting in inhomogeneous temperature distributions (XI)	- More difficult design to fabricate (III)	- Tubes inside phantom can disturb photoacoustic signal (IX) - More difficult design to fabricate (III)
O		- 3D printing can be used to produce the ring - Varying position of holes and hole sizes to increase homogeneous water flow	- Varying position of holes and hole sizes to increase homogeneous water flow
T	- Inhomogneous temperature distribution around surface of phantom, if the flow is not homogeneous (XI)		
Score	5.5	11	10.5

Table 4.2 shows that design 1 has the lowest score. This can be attributed to the fact that the water flow around the phantom is possibly not homogeneous, because of the localized in- and outflow of the water. It is expected that most of the water flows along the upper half of the phantom and not along the lower half. Therefore, the lower half of the phantom is expected to cool down, because heat will be transferred to the water in the imaging bowl, while it is less effectively replaced by new warm water compared to the upper half. This is undesirable because the temperature of the phantom should stay very constant (requirement XI). Designs 2 and 3 are expected to have a more homogeneous water flow and therefore have a higher score. A drawback of design 3 is the position of the tubes inside the imaging field of view, which likely results in a disturbance of the photoacoustic signal. Design 2 is selected as the most promising design since it is expected to have a homogeneous water flow without having disturbing structures in the imaging field of view.

In the next sections, material choices will be made with respect to the tissue-mimicking part (matrix material and PA targets) and the temperature regulation and monitoring.

4.3 Possible materials temperature system

4.3.1 Temperature regulation

According to requirement XI the temperature of the phantom should be very stable and adjustable. The previous section described the design which is based on a water flow system. Systems that can regulate the water temperature in a water bath are e.g. a proportional–integral–derivative controller (PID controller), a hot plate, or a heating pad. The SWOT-analysis for these temperature regulating systems is shown in Table 4.3.

Table 4.3: SWOT-analysis for the temperature regulating system. The characteristics of both temperature controllers are categorised in strengths (S), weaknesses (W), opportunities (O) and threats(T). The corresponding requirement is indicated with a Roman numerals inside parentheses.

	PID controller connected to heating pad	**Hot plate**
S	- Adjustable temperature (X) - Constant temperature, closed loop to compensate for temperature disturbance (XI) - Sufficiently small to transport (IV)	- Adjustable temperature (X) - Contains additional feedback temperature sensor to control hot plate temperature (no temperature overshoot) (XI) - Sufficiently small to transport (IV)
W	- Localized heating, takes time before heat is homogeneously distributed	
O		- Possible to combine with magnetic stirrer for homogeneous temperature distribution
T	- Heating pad has not enough capacity to keep the water at constant temperature (XI)	
Score	9.5	13.5

The hot plate and PID controller both score high on the most important requirements (X and XI) for constant and adjustable water temperature. The hot plate is the best option in this case since the hotplate can be combined with a magnetic stirrer to ensure a more homogeneous water temperature in the water reservoir. This is important since the water in the reservoir will be pumped into the phantom, and the phantom's temperature is required to be as constant as possible.

4.3.2 Temperature monitoring

Requirement XII (Chapter 3) states that the temperature in the tissue-mimicking part (gel wax) should be very constant and therefore monitoring the temperature inside the phantom during the measurements is required. Options to monitor the temperature inside the gel wax are thermocouples, resistance temperature detectors (RTDs), or optical fiber temperature sensors. A SWOT-analysis is made for the different temperature sensors and is shown in Table 4.4.

Table 4.4: SWOT analysis for temperature monitoring inside the phantom. The characteristics of the different temperature sensors are categorised in strengths (S), weaknesses (W), opportunities (O) and threats (T).

	Thermocouple [25]	**PT100 RTD [25]**	**Optical fiber sensors [26]**
S	- Inexpensive - Small measuring tip - Easy temperature logging - Fast response time to temperature changes	- High accuracy (typical accuracy of 0.1°C) - Long term stability and repeatable readings Easy temperature logging	- Fast response - High sensitivity - Optical fibers are made of plastic of glass, and therefore generate less PA disturbance
W	- Generates photoacoustic signal (due to absorbing structures in the NIR range), which can disturb PA images	- Generates photoacoustic signal (due to absorbing structures in the NIR range), which can disturb PA images - Expensive (relative to thermocouples)	- Expensive - sensitive to strain (bending)
O	- Various types (K,T, J etc.) for different temperature ranges		
T	- Less accurate than PT100 RTD (typical accuracy 1°C) - Less stable readings, because of possible chemical changes in the sensor (e.g. oxidation)	- Nearly three times longer response time than thermocouples	- Usable in radio frequency or microwave environments, but unknown how it functions during photoacoustic measurements (using NIR excitation light)
Score	2.5	-0.5	0.5

Thermocouples are considered as the best choice to monitor the temperature inside the tissue-mimicking part of the phantom (see Table 4.4). Thermocouples have the potential to be suitable for measuring the temperature inside the phantom because they have a fast response to temperature changes, have a small measuring tip, and can easily be connected to a data logger to record the measurements. An important threat is that the accuracy might be too low. Inaccurate temperature readings result in an inaccurate speed of sounds which affects the PA reconstructions.

4.4 Possible materials tissue-mimicking part

4.4.1 Matrix material

Currently-used tissue mimicking materials for photoacoustic phantoms include poly(vinyl chloride) plastisol (PVCP), hydrogels such as agarose and gelatine, liquid fat emulsions such as Intralipid, and mineral-oil-based materials such as gel wax. The SWOT-analysis for the matrix materials is shown in Table 4.5.

Table 4.5: SWOT-analysis for matrix material of tissue-mimicking part of the breast phantom. The characteristics of the material are categorised in strengths (S), weaknesses (W), opportunities (O) and threats (T). The corresponding requirement is indicated with a Roman numeral inside parentheses.

	PVCP [27]	**Gelatine/Agarose [28]**	**Intralipid [29, 30]**	**Gel wax [31]**
S	- High stability (> 6 months), and robust (II) - Stability of target position (VII)	- Easy fabrication process (III) - Stability of target position (VII)	- Easy fabrication process (III) - Relatively short time to achieve temperature equilibrium (XI) - Appropriate SOS (1483 m/s in a 1.5% solution) (V)	- High stability (up to 1 year) (II) - Easy fabrication process (III) - Stability of target position (VII) - Appropriate melting point (65 °C) (XIII)
W	- High melting temperature (170-190 °C) - More difficult fabrication process (III) - SOS below the range relevant to breast tissue (1400 m/s) (V)	- Low stability (1-4 months), not mechanically robust (II) - Instability with temperature variations, and low melting points (XIII) - Relatively high SOS for breast tissue (V) (gelatine: 1520-1650 m/s, agarose: 1498-1600 m/s)	- Low stability (homogeneity period of hours and solution reusable for several days) (II) - No stability of target position (VII)	- Difficult to make sure the gel wax is completely free of air bubbles (after pouring it into the mould)
O	- Acoustic attenuation and SOS tunable with plasticisers (V) - Scattering tunable with glass microspheres	- Acoustic attenuation and SOS tunable (e.g with polyethylene, and oil droplets) (V)		- Acoustic attenuation tunable with paraffin wax (V) - Scattering tunable with glass microspheres
T	- Possibly long time to achieve temperature equilibrium (XI)	- Susceptible for microbial invasion	- Leakage	- Possibly long time to achieve temperature equilibrium (XI) - SOS in lower end of the range, and decreasing at higher temperatures (V)
Score	3.5	-1.5	3.5	15

The final scores for each material is calculated as described in Section 4.1 and shown in Table 4.5. Gel wax has clearly the highest score, and is therefore considered as the best choice for the matrix material in the tissue mimicking part of the breast phantom. Gel wax scored high because it possesses many strengths with a high importance factor. Gel wax is a mineral-oil based material that has been previously used for photoacoustic phantoms [31]. Native gel wax is optically transparent and has acoustic properties in the range relevant to breast tissue, see Section **??**. Bakaric *et al* [32] determined the temperature-dependent SOS for native gel wax over a temperature range from 22-40 °C, see Figure 4.4. At room temperature (± 22 °C) the speed of sound in gel wax is 1432 m/s, which is in the lower end of the range relevant to breast tissue. Moreover, the SOS in gel wax decreases linearly if the temperature rises. This might be a threat since in this study the gel wax will be used in a body temperature phantom. The frequency-dependent acoustic attenuation of native gel wax varies from 0.71 dB/cm to 9.93 dB/cm for a frequency ranging from 3 MHz to 12 MHz [31], which falls within the range relevant to breast tissue.

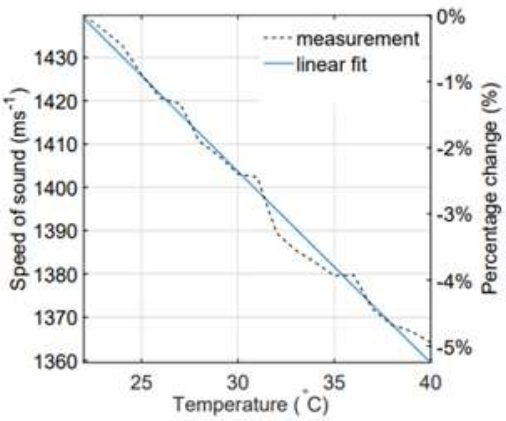

Figure 4.4: Temperature-dependent speed of sound of native gel wax (FF1003, Mindsets Online, Waltham Cross, UK), measured over a temperature range from 22 to 40 °C. Figure from Ref. [32].

4.4.2 Photoacoustic targets

Possibilities for photoacoustic targets are stainless steel microspheres coated with India ink, black epoxy drops, black hairs, or a black leaf skeleton. The SWOT-analysis for those photoacoustic targets is shown in Table 4.6.

All options, except epoxy drops, meet all three aspects of requirement VI (Table 3.1). Table 4.6 shows that the stainless steel microspheres coated with India ink has the highest score. India ink is a particulate absorber, i.e. absorption is caused by insoluble carbon particles in an aqueous medium. The advantage of using ink instead of a molecular dye is that ink particles are not able to diffuse through a gel or polymer matrix. India ink has a smooth absorption spectrum over the NIR region of the spectrum and optical properties of India ink are shown to be stable over a period of at least one year [33]. In the current study, the stainless steel microspheres coated with India ink will be chosen as PA targets, because these microspheres have been successfully used in previous studies [11]. These microspheres showed the opportunity to analyze the resolution in x,y, and z planes by determining the full width half maximum (FWHM) of the point spread function (PSF).

Material choices overview

In this section, several design choices were made with respect to the temperature system and the tissue-mimicking part of the phantom. Concept design 2 seemed to be the most promising design because of the expected homogeneous water flow created by a water in- and output ring. To heat the water flowing through the circuit, a hotplate magnetic stirrer with temperature control was the best option. To monitor the temperature of the phantom, thermocouples appeared to be the best option. The matrix material of the tissue-mimicking part will consist of gel wax, in which stainless steel microspheres coated with India ink will be embedded as PA targets.

Table 4.6: SWOT-analysis for photoacoustic targets in tissue mimicking part of the breast phantom. The characteristics of the targets are categorised in strengths (S), weaknesses (W), opportunities (O) and threats (T). The corresponding requirement is indicated with a Roman numerals inside parentheses.

	Stainless steel microspheres coated with India ink [33]	**Epoxy drops [34]**	**Black hairs [35]**	**Black leaf skeleton [36]**
S	- Strongly absorb all wavelengths of excitation light (VII) - Sub-resolution (360-445 μm) (VI) - Easy positioning, covering the whole field of view - Spherical geometry - Available at UT	- Strongly absorb all wavelengths of excitation light (VI) - Spherical geometry	- Strongly absorb all wavelengths of excitation light (VI) - Sub-resolution diameter ($\pm$ 100 μm) (VI)	- Strongly absorb all wavelengths of excitation light (VI) - Smallest veins are sub-resolution (30 μm) (VI) - Mimicking blood vessel structure - Available at UT
W	- Microspheres are mannualy coated and therefore the ink can be irregularly distributed over the surfaces of the microspheres	- Relatively large size (size ranging from 0.46 - 1.65 mm), not sub-resolution (VI) - Limited positioning, because drops should be positioned on nylon thread	- Cylindrical geometry	- 2D structure - Limited positioning, not covering the whole field field of view
O	- Analyse resolution based on point spread function (PSF) of maximum intensity projections (MIPs) in all 3 dimensions (VI)	- Analyse resolution based on point spread function of maximum intensity projections in all 3 dimensions (VI)	- Analyse resolution based on PSF or line spread function (LSF) of MIP (VI), depending on the orientation of the hairs	-Analyse resolution based on LSF of MIP (VI)
T				
Score	14.5	2.5	11.5	10.5

Fabrication and characterization: Prototype phantom

5

This chapter starts with a description of the design of the prototype phantom. This design is based on the chosen concept design and materials in the previous chapter. Subsequently, the fabrication process of the prototype phantom is described, starting with the production process (materials and methods), followed by presenting the resulting prototype phantom. The chapter continues with the characterization of the prototype phantom, and the results will be discussed.

5.1 Prototype design

In this section, all design choices made in Chapter 4 will be integrated into a prototype design. The prototype design is based on concept design 2, which seemed to be the most promising design based on the SWOT-analysis. Concept design 2 is based on a water flow circuit, covering the surface of the phantom. To realize this idea, a system is designed in which water flows through an interstitial space between two breast-shaped cups made of thin PVC sheets. These cups are currently used during PAMMOTH measurements to stabilize the woman's breast in the imaging bowl [21]. The PVC cups are known to be optically and acoustic transparent and therefore do not disturb the PA measurements [21]. The breast stabilizing cups are available in eight different sizes, starting with size 1 (smallest) up to size 8 (largest). The exact shape and dimensions of the breast stabilizing cups can be found in Ref. [21]. The outermost PVC cup of the phantom is chosen to be a standard cup size 8. The inner PVC cup has a customized size and shape, such that the space between the inner and the outer cup is exactly 2.2 cm. This spacing is chosen, because it is expected that this volume of water between the cups is sufficiently large to remain at a constant temperature when the phantom is placed in the 25 °C water of the PAMMOTH imaging bowl. The dimensions of the two cups are shown in a schematic drawing in Figure 5.1.

Both PVC cups are connected to a hollow ring, such that a system is created through which warm water can flow. The ring consists of two separate half rings of which one half functions as water input and the other as water output. Figure 5.2 shows the dimensions of this water supply ring. The holes in the ring have a varying diameter because a small pressure drop along the ring is expected. To compensate for this pressure drop, the holes are made bigger where the pressure is expected to be lowest such that an equal water flow through the holes is created.

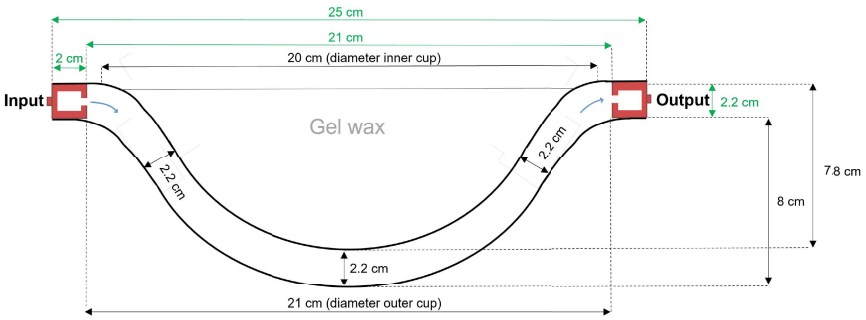

Figure 5.1: Schematic 2D drawing of the dimensions of the prototype design (cross-section). The outer PVC cup has a diameter of 21 cm and a depth of 8 cm. The inner PVC cups has a diameter of 20 cm and a depth of 8 cm. The distance between the PVC cups is 2.2 cm. The dimensions of the water supply ring (drawn in red) are specified in Figure 5.2. The inner PVC cup is filled with gel wax, which is a tissue-mimicking material.

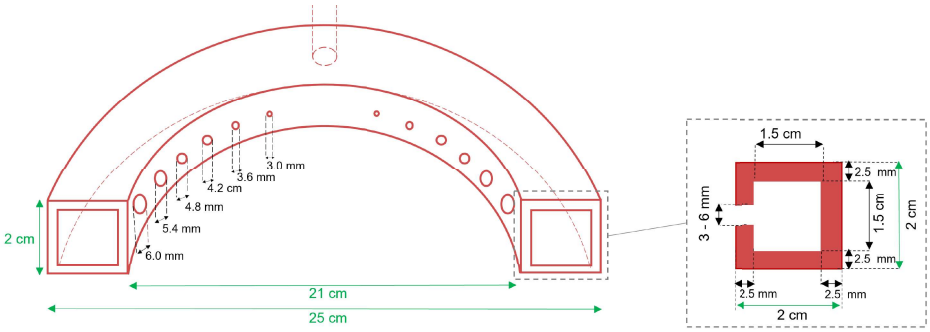

Figure 5.2: Schematic drawing of the water supply ring (cross-section). The ring has an inner diameter of 21 cm and, outer diameter of 25 cm, and a height of 2 cm. The diameter of the holes in the PLA ring linearly vary from 0.3-0.6 cm, depending on the distance from the water input in the back of the ring.

A 3D drawing of the prototype is shown in Figure 5.3. The water supply ring together with the inner and outer PVC cup, form a system through which warm water can flow to ensure the temperature of the phantom can remain at constant temperature. The tissue-mimicking part is placed inside the inner PVC cup and consists of gel wax in which PA targets could be be embedded. However, those PA targets are omitted in the prototype design, since this design will not be used for PA measurements in the PAMMOTH.

Besides the phantom itself, an additional setup is needed to heat the water and to create a water flow through the outer layer of the phantom. A schematic drawing of the total phantom setup is shown in Figure 5.4. The setup consists of a reservoir with water which is heated with a hotplate. The water temperature in controlled via a feedback-loop with a temperature sensor. The pump is place on the input side of the phantom, such that the water from the reservoir is pumped into the input ring. The water flow through the space between the PVC cups, and leaves the phantom via the output ring. The water from the output rings passively flows back into the water reservoir, forming a closed-loop system. The water reservoir, the pump and the phantom are all connected via silicon tubes. The outside of the water supply ring contains two John Guest connector, placed on opposite sides of the ring. These John Guest connectors are connected to a short piece of polyethylene (PE), see Figure 5.4. These PE tubes are rigid and are therefore suitable as connection piece between the John Guest connector and the flexible silicone tubes.

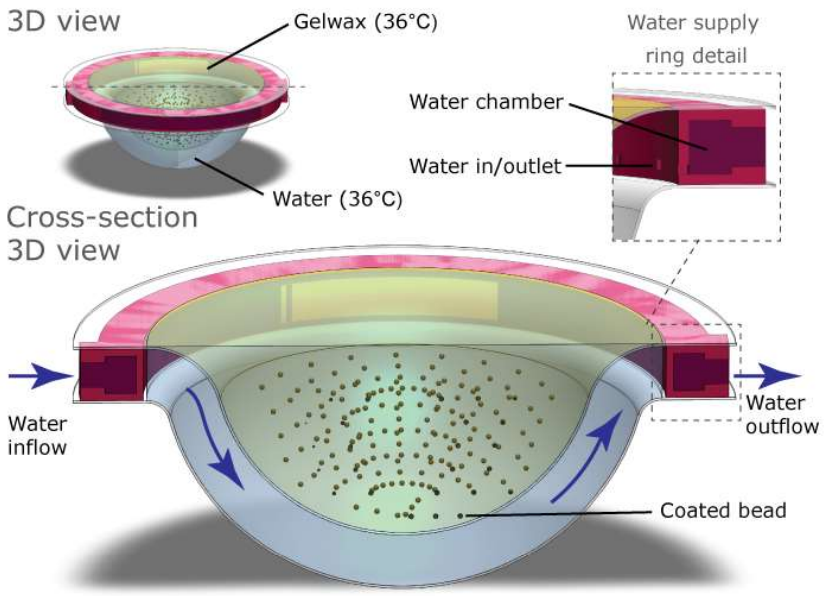

Figure 5.3: 3D drawing of the prototype phantom. Water supply ring (drawn in red) consists of two parts, namely one half functions as a water input and the other half as a water output. The water flows trough two PVC cups which are spaced 2.2 cm. The inner PVC cup is filled with gel wax (tissue-mimicking material) and coated beads (PA targets). Note that in the prototype design these coated beats are not yet included. Solidworks image made by Rianne F.G. Bulthuis.

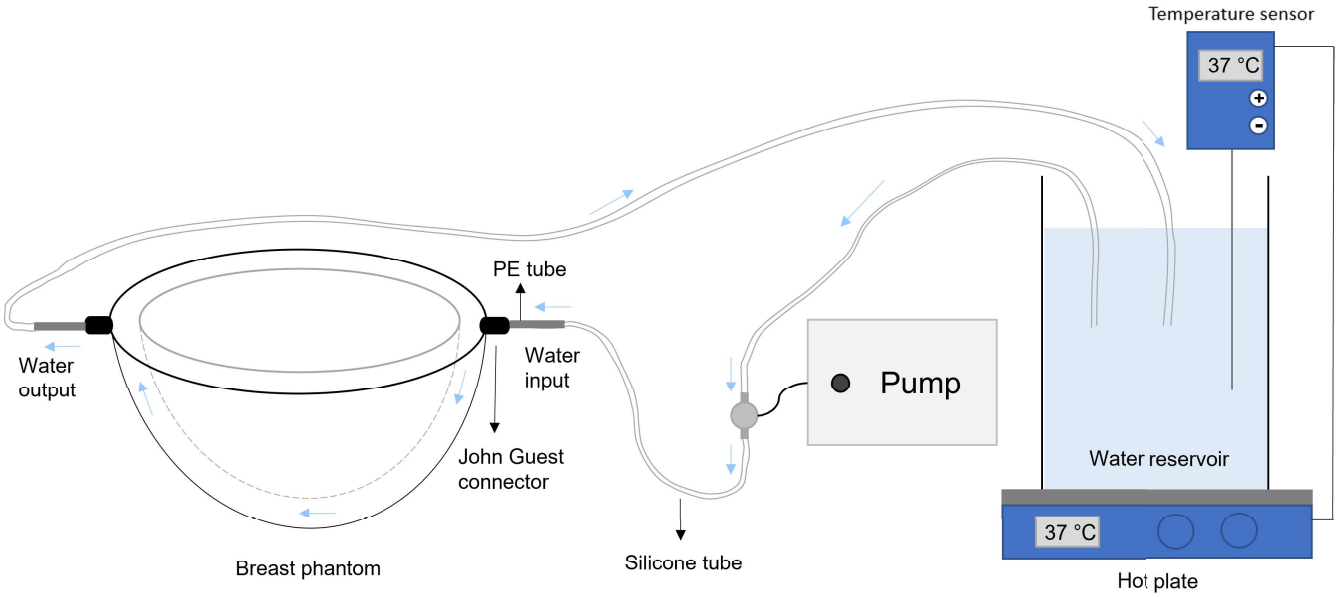

Figure 5.4: Schematic drawing of the total phantom closed-loop setup, consisting of a temperature regulator, a pumping system and the phantom itself. The water in the reservoir is heated with a hot plate and the temperature is maintained at a constant temperature with a feedback-loop with an external temperature sensor in the water reservoir. The warm water is actively pumped trough the space between the PVC cups, thereby heating the surface of the phantom. The water output is passively led back to the reservoir. The tubes connecting the water reservoir, the pump and the phantom are made of silicon.The silicon tubes are connected to the phantom via a piece of polyethylene tube and a John Guest connector.

5.2 Prototype fabrication

In this section, the materials and methods to produce the prototype phantom are described. A brief description of the prototype can be found in Figure 5.3 (Section 5.1). Also the resulting prototype phantom and the flow system setup are shown in this section.

5.2.1 Materials and methods

Production of PVC cups

For the production of the inner and outer PVC cups of the water circuit, a mould to shape the cups was required. The outer cup of the phantom is a standard size 8 breast stabilizing cup [21], which is normally used to stabilize the breast in the imaging bowl. A mould for this cup size was already available. The shape of the outer cup mould is partially defined by an ellipsoid function and partially by a cubic polynomial, details about these functions be found in Ref. [21]. The inner cup has a customized size and shape and therefore a new mould needed to be designed. The shape of the inner cup mould was made in Solidworks such that the space between the inner and outer PVC cup would be 2.2 cm, see Figure 5.5. This cup mould was produced by 3D printing (Ultimaker S5, The Netherlands) with Acrylonitrile butadiene styrene (ABS). Details about the production protocol of the cup mould can be found in Appendix A.1.

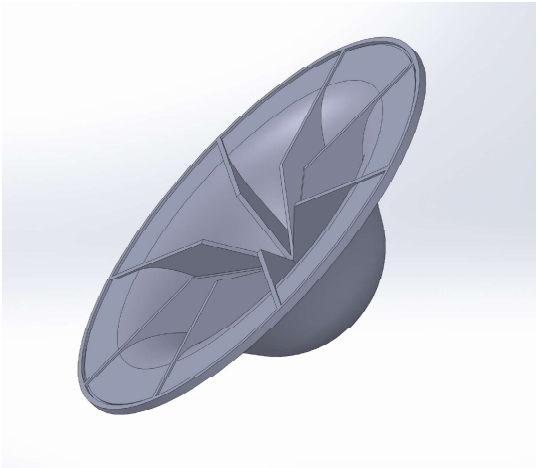

Figure 5.5: Solidworks design of the cup mould for vacuum shaping the inner PVC cup. The height of the cup mould is 7.8 cm and the diameter is 20 cm. The frame on the inside of the cup mould is designed in such a way that all chambers are interconnected, which is required because the vacuum machine only creates a vacuum in the middle of the mould. Design made by Johan C.G. van Hespen.

The inner and outer PVC cups were made from PVC sheets with a thickness of 180 μm. The PVC sheets were shaped into a cup form with a vacuum shaping machine. The PVC sheet was first heated, pressed down onto the cup mould and shaped tightly around the mould by applying a vacuum. Details about vacuum shaping procedure can be found in Appendix A.2

Construction of the water circuit

The water supply ring was 3D printed from polylactic acid (PLA), and the two half rings (input and output) were glued together (Bison, hard PVC-lijm). With a screw tap, a treading was made on the outside of the ring. This treading was used to tightly connect a tube John Guest connector to both half rings. Subsequently, the inner and outer PVC cup were glued to the water supply ring with PVC glue.
To make the total phantom setup shown in Figure 5.4, the phantom was placed in a table with a hole (diameter 21 cm), which has the same size as the aperture in the PAMMOTH imager. Both tube connectors were connected to a short piece (10 cm) of polyethylene (PE) tube with an outer diameter of 10 mm. The PE tubes were in turn connected to silicone tubes with an inner diameter of 10 mm and a length of approximately 0.5-1 m. The closed-loop system was made by connecting the silicone tubes to the phantom, the pump (Micro Pump Controller, Multi-Modality Medical Imaging, University of Twente), and the water reservoir (Erlenmeyer, 3L). The water reservoir was placed on a hot plate magnetic stirrer (IKA® C-MAG HS7) connected to a temperature control sensor (IKA® IKATRON™ ETS-D4). The pump was placed on the table and the water reservoir was placed exactly 30 cm below the table in which the phantom was placed. This allows a passive water outflow from the phantom to the water reservoir. The water from the reservoir was actively pumped towards the phantom, and to ensure equal in- and outflow of the water the pump was set at a pumping speed of 2.80 (arb. unit). The phantom and the silicone tubes needed to be pre-filled with water before the pump was turned on. The volume of water needed to pre-fill the phantom and the tubes was approximately 1 L and the volume of water in the reservoir was approximately 2.5 L.

Production of tissue mimicking-part

The tissue mimicking part of the phantom consists of native gel wax (FF1003, Mindsets Online, Waltham Cross, UK). PA targets are omitted since the prototype phantom will not be used in the PAMMOTH for PA measurements. 1L of native gel wax was first melted inside an oil bath at 150 °C. The inner PVC cup was used as a mould in which the molten gel wax was poured. Meanwhile, the PVC cup was cooled with ice water to prevent deformation of the cup due to the heat of the gel wax.

5.2.2 Fabrication results

The results of the fabricated prototype phantom are shown in this section. Results of testing components of the water circuit, as well as the complete closed-loop setup, are also shown.

Figure 5.6 shows the result of one half of the 3D printed water supply ring made of PLA. The other half ring looked similar. The resulting water flow through the holes is shown in Figure 5.7. The observed volumetric flow rate seemed to increase towards the ends of the half ring, where the diameter of the holes was largest.

The resulting temperature system part of the prototype phantom is shown in Figure 5.8. Filling the system with water went well, until the water level in the phantom had risen above the holes of the output ring. At that moment, air could no longer escape from the phantom, which resulted in bulging of the inner PVC cup, see Figure 5.9. Filling the inner PVC cup with gel wax provided a back pressure that considerably reduced the bulging. However, bulging remained on the periphery of the inner PVC cup that was not covered with gel wax. Also, when the phantom was filled with water, it appeared to be mostly watertight. There was no leakages between the water supply ring and the PVC cups, meaning that the PVC glue ensures a sufficiently strong and watertight connection.

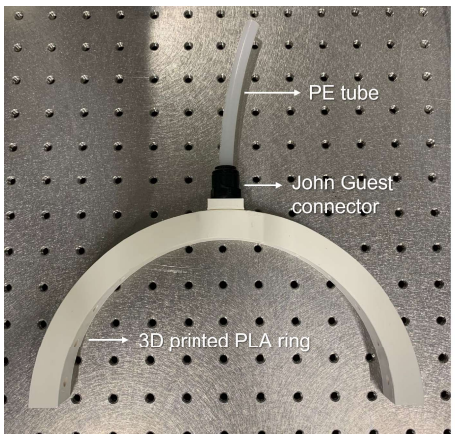

Figure 5.6: Top view of the 3D printed printed water supply ring made of PLA. The outside of the ring is connected to a John Guest connector which is in turn connected to a polyethylene (PE) tube.

Figure 5.7: Image of the water supply ring being tested with water. The volumetric flow rate differed per hole size.

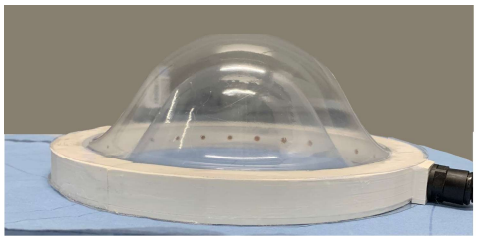

Figure 5.8: Side view of the temperature system part of the phantom, consisting of the water supply ring, the inner PVC cup and the outer PVC cup. The distance between the inner and outer PVC cup is 2.2 cm.

Figure 5.9: Image of the prototype phantom without gel wax in the inner PVC cup. When the phantom was filled with water, the excess air could not escape from the phantom and this resulted in bulging of the inner PVC cup. The arrow points to the part of the phantom that is filled with air.

Figure 5.10 shows the resulting phantom closed-loop setup in the lab. For smooth functioning of the flow through the closed-loop system, the elevation of the water reservoir relative to the phantom was crucial. The elevation of the reservoir had to be chosen such that the rate of the passive outflow matched the pumping rate that regulated the inflow rate into the phantom. When the reservoir was placed too high, there was no passive outflow and the water accumulated inside the phantom, resulting in a pressure build-up.
Also, when testing the phantom setup with water, a lot of tiny gas bubbles were formed and adhered to the surface of the inner PVC cup, see Figure 5.11. These gas bubbles might become a problem during the PA measurements since ultrasound could be reflected by the surface of gas bubbles or attenuated when going through the bubbles.

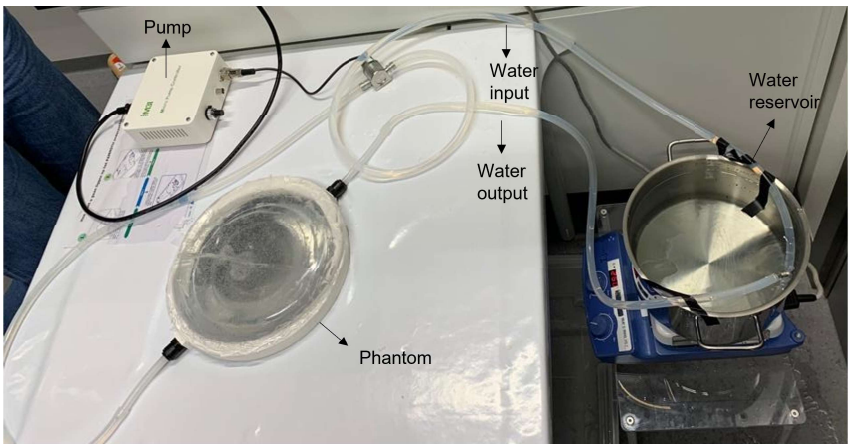

Figure 5.10: Phantom closed-loop setup in the lab. The phantom is connected to the pump and the water reservoir via silicone tubes. The hotplate and the water reservoir were placed 30 cm below the table to allow passive water outflow. In this setup, a pan was used as a water reservoir and a temperature control sensor was absent.

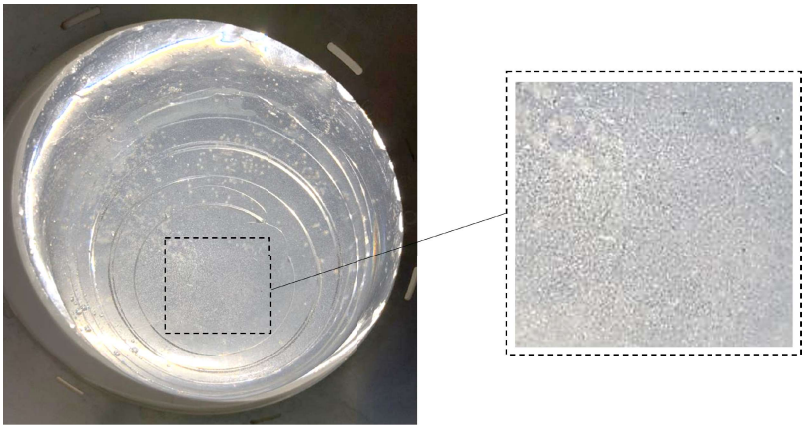

Figure 5.11: Bottom view of the concept phantom filled with water. When the water flows trough the closed-loop system, tiny gas bubbles adhere to the surface of the PVC cups.

5.3 Prototype characterization

Requirement XI states that the phantom should have a stable and homogeneous temperature. In this characterization experiment, it will therefore be investigated to what extent the temperature of the gel wax, initially at room temperature, changes when warm water (body temperature) is flowing through the water circuit around the surface of the phantom.

5.3.1 Materials and methods

Gel wax temperature stability

The measurement setup used for this experiment is the total phantom setup described in Section 5.2.1. Additionally, three K-type thermocouples (XTVTX) were placed inside the gel wax, in such a way that the appearance of a horizontal temperature gradient in the gel wax could be measured. Figure 5.12 shows the exact position of the thermocouples. It was chosen to place the thermocouples only in the top part of the phantom to be comparable

with the gel wax temperature measurements during a PA measurement in the PAMMOTH. For PA measurements the thermocouples need to be placed high, to minimize the disturbing photoacoustic signal from the thermocouples in the PA images. Each thermocouple was connected to a voltage-temperature converter (National Instruments, USB-TC01). The data was logged with the smallest sample rate possible, which was 1 Hz. The hot plate was set to heat the water to 37 °C. The highest temperature in the range of breast skin temperatures (33-37 °C [12]) was chosen, because this gives the maximum temperature difference between gel wax (room temperature) and the water flowing through the circuit, hence the heat transfer rate is highest. The water was pumped through the water circuit around the surface of the phantom and the temperature inside the gel wax was measured until thermal stability was reached at all three positions.
The measured data was plotted in a temperature-time diagram as a minute averaged temperature. This was done by first smoothing the data with a moving average with a span size of 60 seconds, and subsequently plotting the temperature once per minute by downsampling the data.

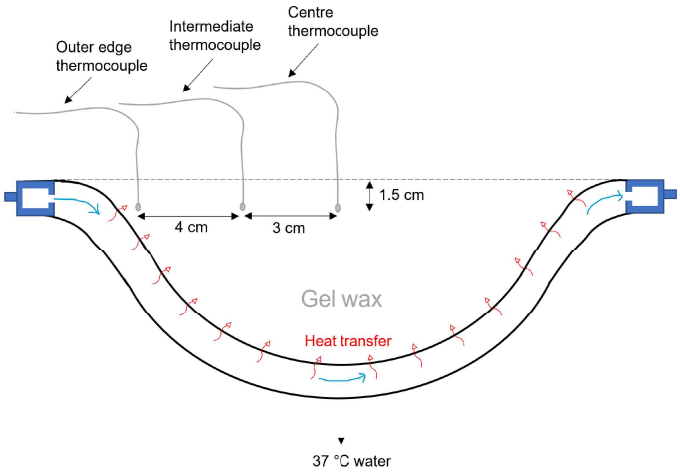

Figure 5.12: Schematic 2D drawing of the phantom with three K-type thermocouples to measure the horizontal temperature gradient inside the gel wax over time. The first thermocouple is placed in the centre, the second thermocouple is placed at a radius of 3 cm from the centre thermocouple, and the third thermocouple is placed very close to the inner PVC cup at a radius of 7 cm from the centre thermocouple. All thermocouples are placed at a depth of 1.5 cm in the gel wax.

5.3.2 Characterization results

Gel wax temperature stability

The temperature-time diagram resulting from the temperature monitoring inside the gel wax is shown in Figure 5.13. The start temperature of the gel wax was 23.3 °C at all three positions. The thermocouple at the outer edge shows an offset of 7 °C because the recording of the temperature started after filling the water circuit and setting up the closed-loop system. The temperature at the outer edge of the gel wax reached a constant temperature of 37 °C after approximately 2.5 hours (150 minutes). The measured fluctuations in the gel wax at the outer edge are due to temperature fluctuations of the water in the reservoir. The cause of these fluctuations was a defect in the feedback loop of the hot plate and temperature sensor, and therefore the temperature of the hot plate needed to be manually adjusted to keep the temperature of the water in the reservoir constant. The measured temperature in the gel wax at the centre and intermediate position were lower than the gel wax temperature at the outer edge, indicating that there was a horizontal temperature gradient inside the gel wax. After 220 minutes (3.7 hours) the gel wax

at the intermediate and centre position was still increasing and still deviated from the temperature at the outer edge.

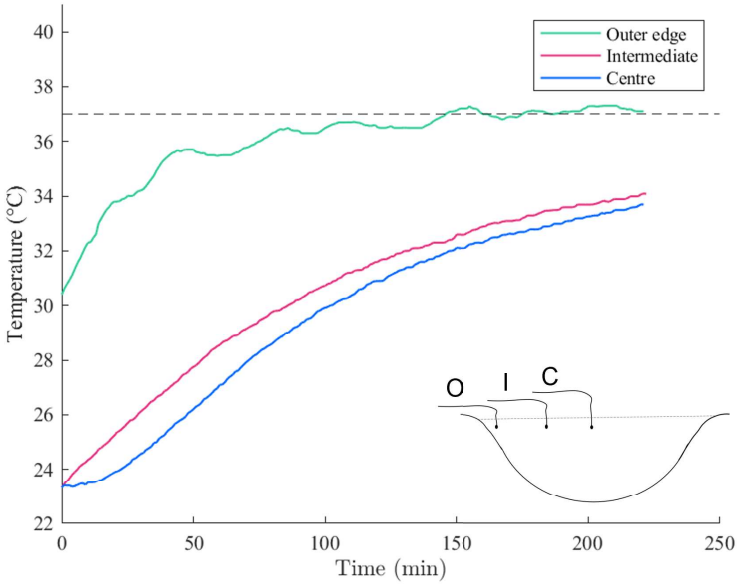

Figure 5.13: Temperature-time diagram of the temperature stability inside the gel wax during 37 °C water flow through the water circuit. The temperature inside the gel wax is measured with thermocouples at three positions, namely at the centre (C), at intermediate position (I) and at the outer edge (O), as indicated in the graph inset.

5.4 Discussion and conclusion

The increasing diameter of the holes towards the ends of the half ring was supposed to compensate for the expected small pressure drop along the ring. However, since the volumetric flow rate was not equal for all holes, the compensation with varying hole sizes was unsuccessful. This could mean that there is no significant pressure drop because the resistance of the holes is much higher than the resistance of the water channel. Another possible explanation is that the hole sizes are incorrectly scaled to compensate for the pressure drop. The diameter of the holes increased linearly, however linearly scaling the surface area of the holes could have led to more appropriate compensation of the volumetric flow of water through the holes.

Aside from the bulging induced by the air trapped between the PVC cups, the general idea of creating a closed-loop pumping system appeared to work, provided that the water inflow and outflow are well balanced.

An explanation for the formation of tiny bubbles is that water contains dissolved gasses such as oxygen, nitrogen, and carbon dioxide. The bubbles may have formed by diffusion of these gasses into the surface imperfections of the PVC cup. This process is called heterogeneous nucleation [37] and takes place when the water is supersaturated.

The gel wax characterization measurement showed that the gel wax temperature does not remain stable when warm water flows through the water circuit around the surface of the phantom. Heat from the water is transferred to the gel wax which causes an unstable and inhomogeneous temperature distribution inside the gel wax. Waiting for the gel wax to stabilize at a constant and homogeneous temperature, equal to the water temperature, was

shown to take hours. Considering this, requirement XI is not met and therefore a modification is needed to make the phantom suitable for PA measurements in the PAMMOTH.

Recommendations for modifications

To improve the functionality prototype design, several modifications need to be made. Recommendations for those modifications are proposed and listed below.

- To improve the homogeneity of the water supply ring, only one hole size could be chosen. The smallest hole size (diameter 3 mm) already showed sufficient water output.
- To diminish the amount of air captured in the phantom, the holes in the water supply ring could be placed higher.
- To oppose bulging of the inner PVC cup, extra back pressure could be provided by adding an extra layer of gel wax, which also covers the periphery of the PVC cup.
- To solve the problem of the tiny gas bubbles adhering to the PVC cups, the water could be degassed before use. Water can be degassed with several methods, of which a straightforward method is cooking the water (thermal regulation). Cooking the water reduces the amount of gas because less gas can dissolve in liquids at higher temperatures.
- To prevent the thermal gradient inside the gel wax due to heat transferred from the warmer water, the gel wax could be pre-heated to the same temperature as the water in the water circuit around the surface of the phantom, such that no temperature difference is present and therefore no heat is transferred. Moreover, the top part of the gel wax could be isolated to prevent heat loss to the surroundings.
- To improve the stability of the water temperature in the reservoir, another hotplate and temperature control sensor should be used, because the currently used devices did not function properly due to technical errors.

Fabrication and characterization: Final phantom

6

In Chapter 5, a prototype phantom was developed, tested, and evaluated. The general idea of creating a water flow through the surface of the phantom with a closed-loop pumping setup seemed to work fine. Still, some improvements are necessary to make the phantom suitable for PA measurements in the PAMMOTH imager. A final phantom is designed in which several modifications were made with respect to the prototype phantom (see recommendations in Section 5.4). This chapter discusses the design, fabrication, and characterization of the final phantom.

6.1 Final phantom design

The design of the final phantom, including the closed-loop setup, remained largely the same as the prototype phantom. Only the design of the water supply ring was adapted based on the recommended modifications in Section 5.4.

A new water supply ring was designed and is shown in Figure 6.1. This ring contains square holes with a size of 3x3 mm, which were placed at a higher position in the ring compared to the prototype design. The shape of the holes was changed from round to square, to create a larger surface area close to the top of the ring through which air can escape. Moreover, a raised edge is added to the water supply ring, which enables the addition of extra gel wax. The dimensions of the new ring are shown in Figure 6.2. Additionally, a styrofoam (polystyrene) disc was placed on top of the gel wax layer for the purpose of insulation, for which the need is discussed in Section 6.4.

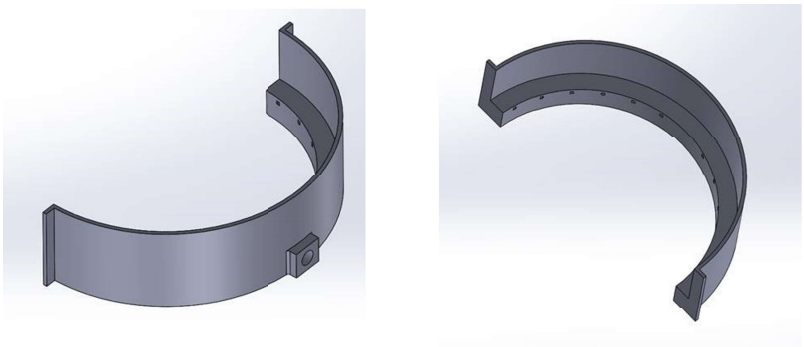

Figure 6.1: Solidworks drawing of the new design for the water supply ring. Both half rings contain twelve square holes with a size of 3x3 mm. The holes are placed in the upper part of the ring. A raised edge is added to the ring to enable the addition of extra gel wax. The inner diameter of the ring is 21 cm, the outer diameter is 25 cm and the height is 6.5 cm. Drawing made by Johan C.G. van Hespen.

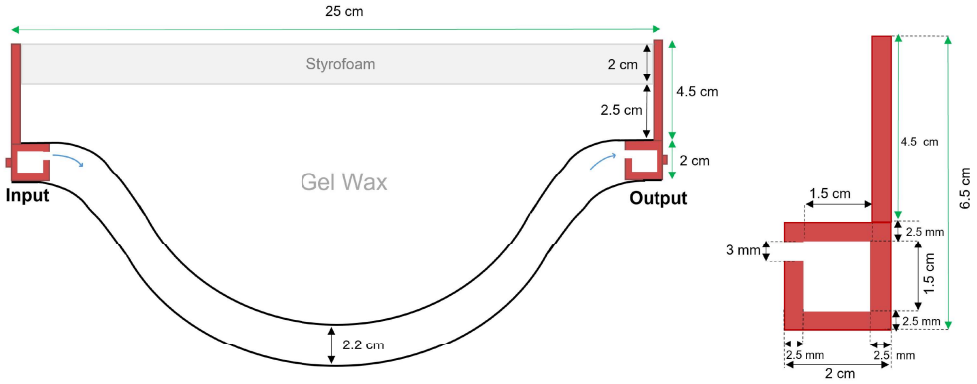

Figure 6.2: Schematic 2D drawing of the dimensions of the ring for the final design. The dimensions of the ring remained unchanged compared to the prototype design (see Figure 5.2), but the size and position of the holes in the ring are changed and a raised edge of 4.5 cm height is added to the ring. A styrofoam disc is placed on top of the gel wax part for insulation.

6.2 Final phantom fabrication

In this section, the fabrication methods of the final phantom are described and the results of the final phantom will be shown. The fabrication methods largely overlap with the fabrication of the prototype phantom. However, the fabrication of the tissue-mimicking part for the final phantom differs from the prototype phantom.

6.2.1 Materials and methods

Production of the PVC cups

The fabrication of the PVC cups for the water flow circuit was the same as previously described in Section 5.2.1.

Construction of the water circuit

The fabrication of the water circuit was the same as previously described in Section 5.2.1. Except, the newly designed water supply ring was used. Also, the construction of the closed-loop setup remained unchanged.

Production of the tissue-mimicking part

The tissue mimicking part of the final phantom consists of gel wax in which PA targets are embedded. The production protocol is described below.

Native gel wax (FF1003, Mindsets Online, Waltham Cross, UK) was first melted in a glass beaker inside an oil bath at 150 °C under regularly stirring. Subsequently, degassing of the melted gel wax was performed in a vacuum oven (Herasus) at 100 °C until air bubbles were absent with visual inspection. The inner PVC cup was used as a mould in which eight layers of gel wax of 1 cm thickness were poured one by one, see Figure 6.3. The volumes of gel wax of each layer varied from 16 mL for the first layer (bottom of the cup) to 158 mL for the eighth layer (top of the cup) to ensure equal layer thickness. The PVC cup was cooled with ice water to prevent deformation of the cup due to the heat of the gel wax. The gel wax was poured carefully into the inner PVC cup using a glass funnel to

prevent the formation of new air bubbles. Each layer had to solidify for approximately 10 minutes, but after the first 1.5-2 minutes the PA targets were distributed by hand over the surface of the gel wax layer. The PA targets used were stainless steel microspheres (Coshperic LLC, United States) with a diameter of 360-445 μm, that were manually coated with undiluted India ink (Royal Talens, The Netherlands). The details of the coating protocol can be found in Appendix B. In total 127 PA targets were distributed over the eight layers. The advantage of casting gel wax in layers is the equal distribution of PA targets throughout the gel wax, which facilitates later analysis of the targets in PA reconstructions. When the cup was filled with the eight layers of gel wax, an extra layer of gel wax (2 cm) was added on top of the inner cup. Degassing of this gel wax was not required, because this extra layer is out of the field of view of the PAMMOTH imager. More details for the native gel wax preparation and casting of the gel wax can be found in Appendix C.

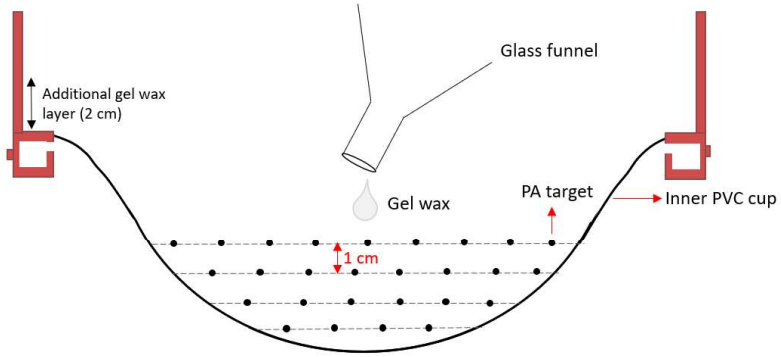

Figure 6.3: Schematic 2D drawing of the production procedure of the tissue-mimicking part. Gel wax was poured into the inner PVC cup layer-by-layer. On top of each layer multiply PA targets (stainless steel microspheres coated with India ink) were distributed by hand. All layers had a thickness of 1 cm, and in total 8 layers were used to fill the phantom. An additional gel wax layer of 2 cm was added on top of the inner cup. The outer cup is omitted in this drawing for simplicity.

6.2.2 Fabrication results

The resulting final phantom is shown in Figure 6.4. The final phantom was tested in the same way as the prototype design. The equal hole sizes in the water supply ring resulted in a more homogeneous water flow out of the ring. Also, the bulging of the inner PVC cup due to captured air was absent, and only small air bubbles remained in the top part of the phantom, see Figure 6.5. The use of degassed water largely reduced the amount of tiny gas bubbles adhering to the PVC cups.

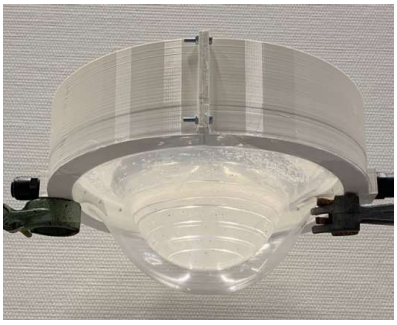

Figure 6.4: Image of the final phantom (side view).

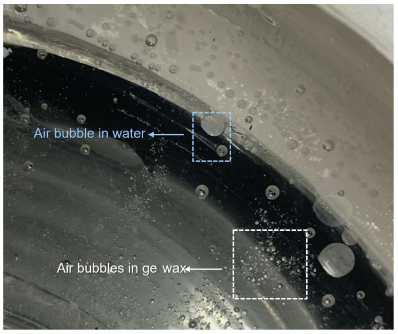

Figure 6.5: Close-up picture of the phantom (top view) showing air bubbles. The small air bubbles (white box) are inside the top layer of gel wax and the larger air bubbles (blue box) against the edge of the ring are inside the water between the PVC cups.

6.3 Final phantom characterization

This section starts with describing the methods to characterize the thermal stability and homogeneity of both the water layer and the gel wax of the final phantom. Subsequently, the results are shown and will be discussed. An overview of the characterization experiments is shown in Table 6.1.

Table 6.1: Overview of the experiments (1-4) to characterize the phantoms thermal stability and homogeneity. Specifications describe the used materials for characterization (IR camera and/or thermocouples) and the setup used for the characterization (either in the lab or in the PAMMOTH at the MST hospital in Oldenzaal).

Exp.	Description	Specification
1A	Water layer temperature homogeneity (without flow)	IR camera, lab setup
1B	Water layer temperature homogeneity (with flow)	IR camera, lab setup
2	Water layer temperature stability	Thermocouples, PAMMOTH
3	Gel wax temperature stability and homogeneity	IR Camera and thermocouples, PAMMOTH
4	Gel wax temperature stability with 25 °C water layer	IR Camera and thermocouples, PAMMOTH

In Figure 6.6 a heat flux diagram is shown, to visualize the heat transfer processes that can occur when the phantom is placed inside the PAMMOTH. Understanding these heat fluxes can contribute to the interpretation of the results presented in this section.

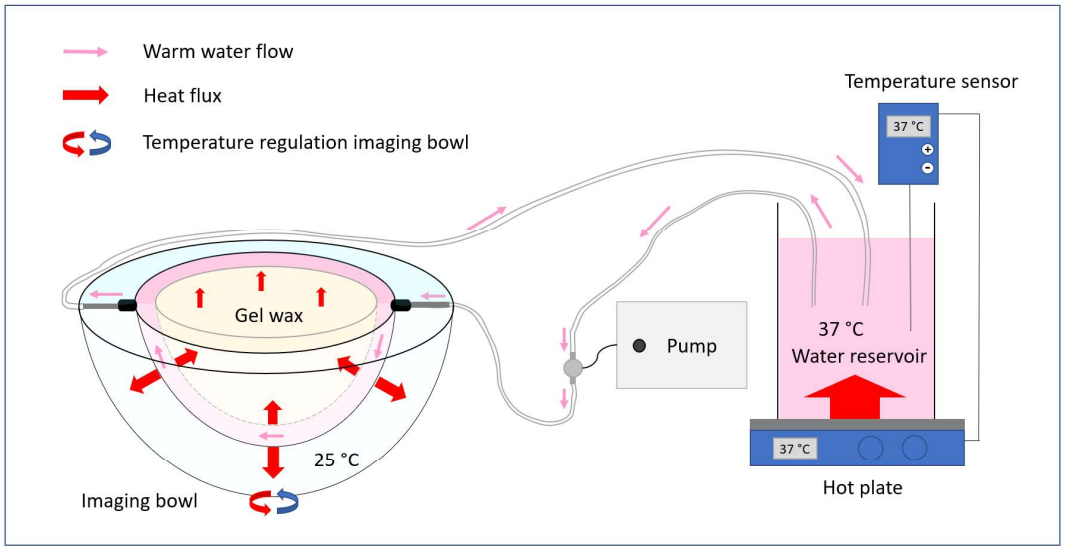

Figure 6.6: Heat flux diagram for the total phantom setup when placed in the PAMMOTH imaging bowl. The water in the reservoir is heated to a set temperature in the range of body temperature. While the water flows through the surface of the phantom, heat is transferred to the cooler water in the imaging bowl. Heat is also transferred to the gel wax, provided that the gel wax is cooler than the water in the water layer. If the gel wax is pre-heated to an equal temperature as the water flowing through the surface, in principle no heat will be transferred. If the top part of the gel wax is not isolated, some heat will be transferred to the surroundings. To reach thermal stability in the system, the heat influx (hot plate) should balance with all heat losses.

6.3.1 Materials and methods

Thermocouple calibration

It is required to calibrate the thermocouples before use, such that every thermocouple gives an accurate temperature output. In the following experiments, K-type thermocouples (XTVTX) connected to USB-TC01 converters (National instruments) were used. The calibration procedure and the calibration curves can be found in Appendix E.

Experiment 1: Temperature homogeneity - phantom water layer

The phantom set-up used to investigate the homogeneity of the phantom's surface temperature is the closed-loop setup, as described in Section 5.2.1 and Figure 5.4. A thermographic (IR) camera (Optris PI 450i) was used to make real-time thermographic images of the phantom's surface with an accuracy of $\pm$ 2 °C or $\pm$ 2 % (whichever is greater). The thermal camera was placed underneath the table in which the phantom was placed (see Figure 6.7), such that the surface of the phantom was in the field of view of the camera.

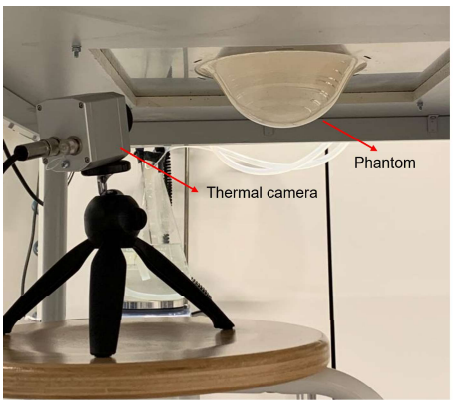

Figure 6.7: Thermal camera setup. The camera is placed underneath the table in which the phantom is placed such that the surface of the phantom is in the field of view of the thermal camera.

The first measurements (experiment 1A) aimed to demonstrate the effect of flowing water compared to standing water on the surface temperature homogeneity. The used setup is described in Section 5.2.1 was used, but the pump was turned off and the silicone tubes were constricted such that the phantom was filled with standing water of 37 °C. The surface temperature of the phantom was recorded with the IR camera for approximately 1 minute. This measurement was done with the phantom in air. The measurement was repeated with the phantom placed in a bowl with 25 °C water, mimicking the PAMMOTH imaging bowl. The surface temperature of the phantom was measured after 5 minutes with the thermal camera. Before the measurement started the bowl with 25 °water was taken away and the surface of the phantom was wiped to remove droplets. After the measurement, the phantom was placed back in the bowl with new 25 °C water. In total 4 repeated measurements of 5 minutes were done.

For the next measurement (experiment 1B), the pumping system was turned on causing 37 °C water to flow through the water circuit around the surface of the phantom. The same measurement procedure was followed as described above, except the surface temperature of the phantom was measured every 10 minutes and in total six repeated measurements were done. The measurement interval was longer because the cooling rate was expected to be lower because of the continuous inflow of new warm water.
The results were analyzed in Matlab to establish the homogeneity of the surface temperature. For each measurement, a snapshot of the thermal camera data was taken in the first 10 seconds after removing the 25 °water bath. The homogeneity of the surface temperature was evaluated by selecting twelve square sampling areas (15x15 pixels) in each snapshot. For each sampling area, the mean and standard deviation of the 225 temperature values was calculated.

Experiment 2: Temperature stability - phantom water layer

The phantom's closed-loop setup was made as described in Section 5.2.1 and Figure 5.4, except the phantom was placed in the imaging bowl of the PAMMOTH instead of the table in the lab. Also, another hot plate (IKAMAG RET-G) was used, as recommended in Section 5.4. The hot plate was set to maintain the temperature of the water in the reservoir at 36 °C. This temperature was chosen because this experiment was simultaneously conducted with experiment 3. The phantom was first placed inside the imaging bowl of the PAMMOTH and subsequently, the bowl was filled with 25 °C water. The recirculation speed of the water in the imaging bowl was set at its minimum value, to be comparable to the situation during a patient PA measurement. The temperature stability of the water flowing through the phantom was evaluated by continuously measuring the temperature of the water in the reservoir with a

PT100 resistance thermometer connected to a data logger (Pico Technology, PT-104, Great Britain). The sampling frequency was set to 1 Hz and the measured data was visualized in a temperature-time diagram.

Experiment 3: Gel wax temperature stability and homogeneity

Four thermocouples (XTVTX) were placed inside the gel wax to investigate how the temperature inside the gel wax changes over time. The thermocouples were positioned in such a way that the temperature gradient in the gel wax could be monitored in vertical and horizontal directions, see Figure 6.8. More thermocouples were used compared to the measurements in the prototype phantom, to get a more complete characterization of the gel wax stability. The phantom was first pre-heated in a water bath of 45 °C for approximately 2.5 hours to reach a constant and homogeneous gel wax temperature before the start of the measurement. A more detailed description of the pre-heating procedure can be found in Appendix D. This experiment was conducted simultaneously with experiment 2, and therefore the used phantom setup in the PAMMOTH is the same. The hot plate (IKAMAG RET-G) was used was set to maintain the temperature of the water in the reservoir at 36 °C. This temperature was equal to the temperature of the pre-heated gel wax, and therefore should in theory prevent the formation of a thermal gradient inside the gel wax. The temperature of the gel wax is monitored continuously for 100 minutes with the four K-type thermocouples at a sampling frequency of 1 Hz. Moreover, a thermal camera was placed above the phantom to measure the surface temperature of the gel wax during the first 50 minutes, see setup in Figure 6.9. A temperature measured by the thermal camera was converted to a temperature-time diagram by defining a one sampling area covering the gel wax surface. After 50 minutes, the phantom's top surface was isolated with styrofoam to minimize heat loss from the gel wax.

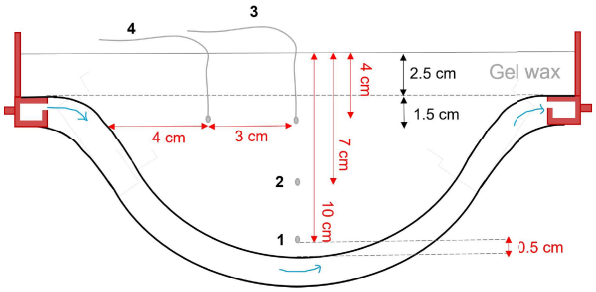

Figure 6.8: Schematic 2D drawing of the phantom with four K-type thermocouples to measure the horizontal and vertical temperature gradient inside the gel wax over time. The wire of thermocouple 1 and 2 is omitted for clearity.

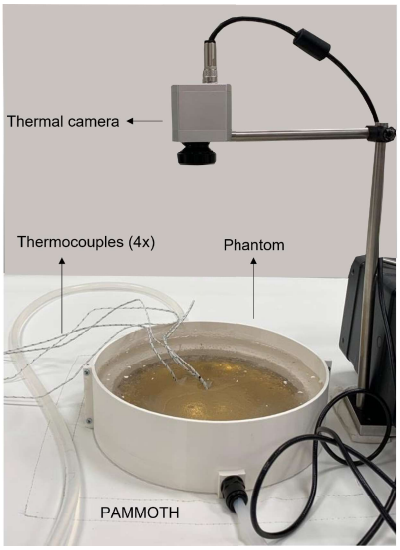

Figure 6.9: Image of the setup used to characterize the thermal stability and homogeneity of the gel wax in the phantom. The thermal camera

Experiment 4: Gel wax temperature stability with 25 °C water layer

The last experiment was conducted to investigate how fast pre-heated gel wax started to cool down inside 25 °C water. Exactly the same setup was used as described in experiment 3, except the temperature of the water in the reservoir was set to 25 °C water and the measurement time was 15 minutes.

6.3.2 Characterization results

Experiment 1A: Temperature homogeneity - phantom water layer without flow

The effect of placing the phantom with standing water of 37 °C inside a cooler environment of 25 °C water (mimicking the PAMMOTH) was determined with the thermal camera. The thermal images of the phantom measured over a time period of 15 minutes are shown in Figure 6.10. The biggest change in temperature is observed after the first five minutes. The surface of the phantom is coolest at the bottom and hottest at the top, which can be explained by the fact that cold water is denser than hot water. The average surface temperature of the phantom decreased over time and the temperature distribution became more inhomogeneous and shifted more towards cooler temperatures, see Figure 6.10.

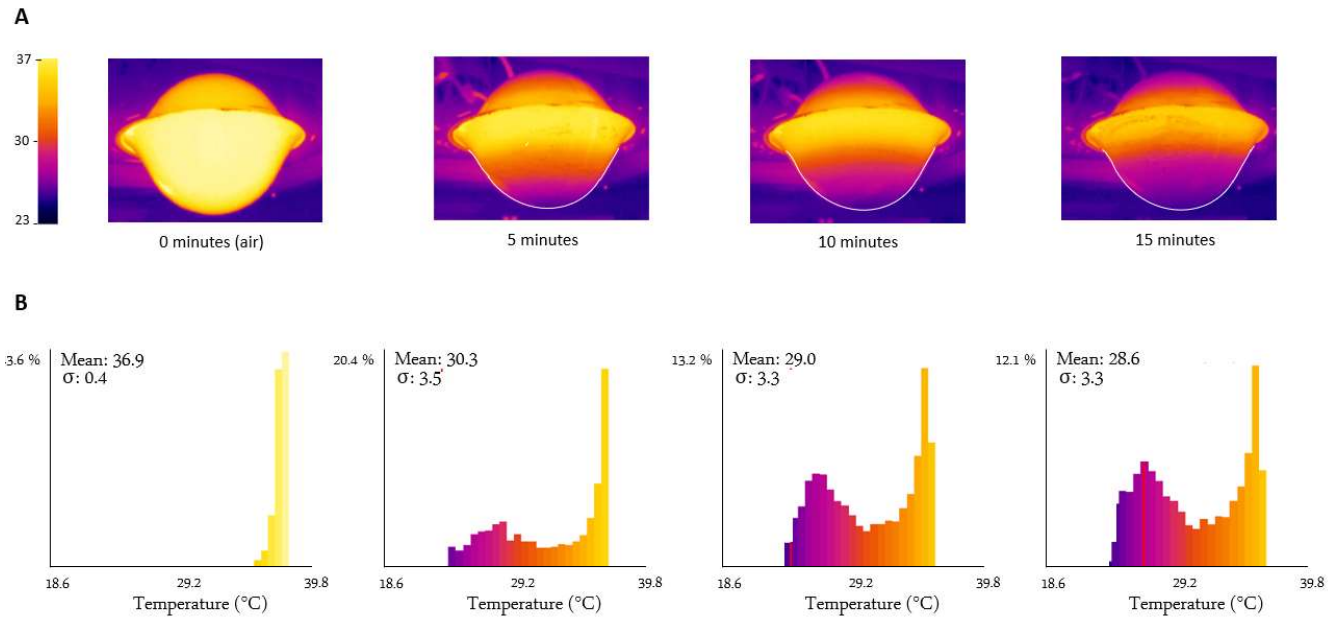

Figure 6.10: ***A****) Thermal camera images of the phantom without flowing water. Before the measurement (0 minutes) the phantom was filled with 37 °C water. During the measurement, the phantom was placed in a 25 °C water bath and after 5, 10, and 15 minutes the phantom's surface was measured with the thermal camera. The hemisphere above the phantom is a thermal reflection on the metal plate underneath the table in which the phantom was placed.* ***B****) Histograms corresponding to the images thermal images. The average temperature decreases over time and temperature distribution shifts more towards cooler temperatures. The standard deviation is used to (σ) indicate the measure of spread in temperatures.*

Experiment 1B: Temperature homogeneity - phantom water layer with flow

Thermal camera images revealed homogeneous temperature over the surface of the phantom with flowing water, as illustrated by Figure 6.11. Snapshot images of the other measurement times looked similar, see Figure 6.13. Histograms of the surface area temperature all looked comparable to the left histogram in Figure 6.10B. The mean surface temperatures in the twelve sampling areas ranged between 35.4 and 36.4 °C, see figure 6.12. There is an obvious difference between the sampling areas in the centre (red boxes) and on the periphery (blue boxes) of the surface. The mean temperatures of the areas in the periphery area are lower than those in the central areas, and the standard deviations are clearly larger. The same observations hold for the other five measurement times (for 0 minutes, 30-60 minutes). The graphs with mean temperature and standard deviation of those measurements can be found in Appendix F.

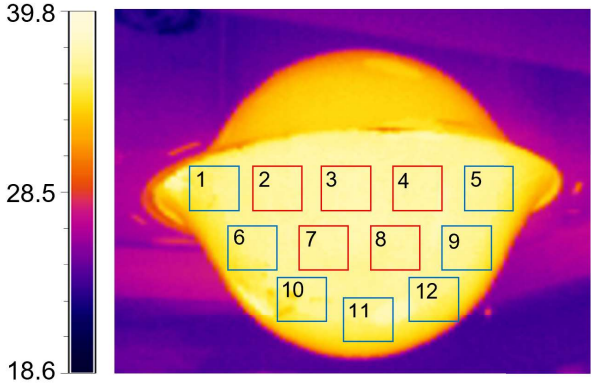

Figure 6.11: Snapshot of thermal measurement in experiment 1 after 20 minutes. The squares indicate the position of the surface temperature sampling areas.

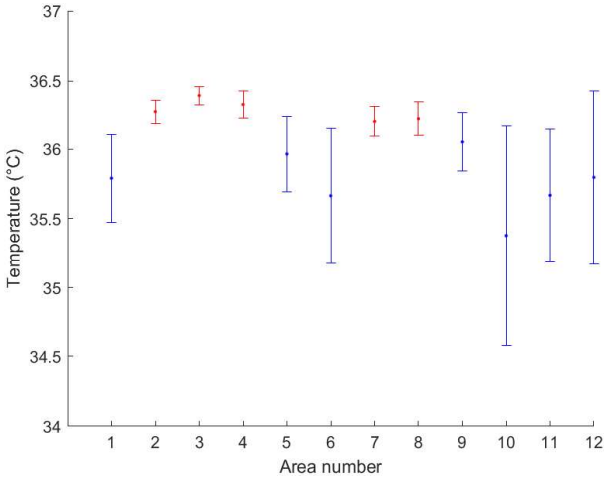

Figure 6.12: Mean and standard deviation of surface temperature in each sampling area (see Figure 6.11) for experiment 1B after 20 minutes.

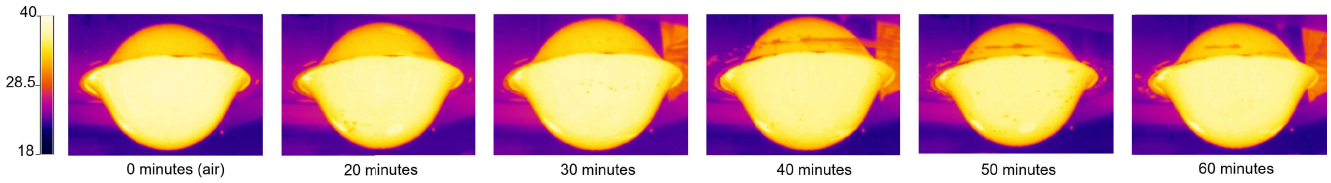

Figure 6.13: Snapshots of thermal measurements in experiment 1 after different time periods from 0-60 minutes. The first measurement shows the phantom's surface temperature when the phantom was placed in air (before start of experiment). The other five measurements show the phantom's surface temperature after a particular time in a 25 °C water bowl. The measurement after 10 minutes is omitted since the water level in the bowl was too low. The mean and standard deviation graphs of the 12 sampling areas of these measurements can be found in Appendix F.

Experiment 2: Temperature stability - phantom water layer

The stability of the temperature in the phantom's water layer was determined by analyzing the temperature stability of the water in the reservoir. In air, the water temperature of the phantom remained constant at 35.6 °C. When the phantom's surface came into contact with the 25 °water in the imaging bowl, the temperature of the water in the reservoir started to decrease. After 12 minutes the water temperature stabilized at 33.7 °C, see Figure 6.14.

After 21 minutes the set temperature of the hot plate was manually changed from 36 to 40 °C to increase the water temperature back to the start temperature. The temperature started to increase but large fluctuations were present. Those temperature fluctuations were caused by the temperature feedback loop between the hot plate and the temperature sensor in the water reservoir. A possible explanation for this is given in Section 6.4. Approximately 40 minutes after changing the set temperature, the temperature of the water stabilized at 35 °C, although this was lower than the indicated set temperature of 40 °C.

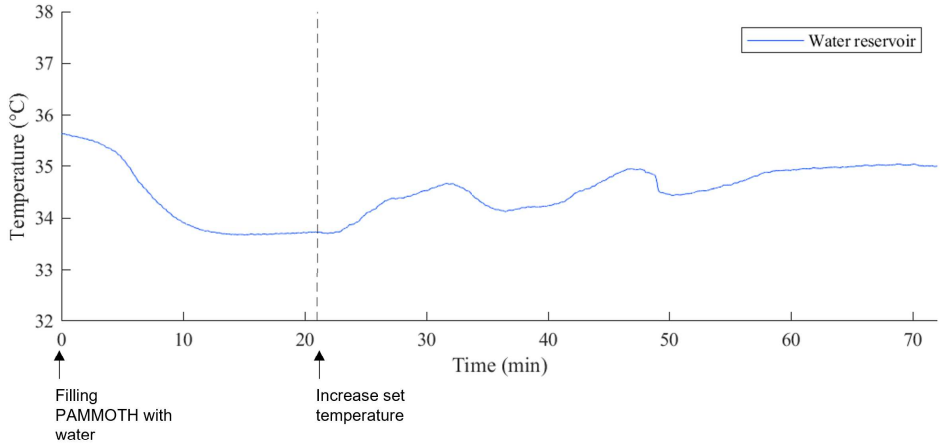

Figure 6.14: Temperature-time diagram of the water temperature measured in the reservoir. At the start of the measurement, the imaging bowl was filled with 25 °C water. After 21 minutes, the hot plate settings were changed to increase the temperature of water in the reservoir.

Experiment 3: Gel wax temperature stability and homogeneity

An overall trend observed is that the pre-heated gel wax cooled down slowly over the duration of the experiment, see Figure 6.15. The typical cooling rate for thermocouples 3 and 4 was only 0.03 °C/min and for thermocouples 1 and 2 this is even smaller. It is noticeable that the top part of the gel wax (thermocouples 3 and 4 and the thermal camera) cooled at a slightly higher rate than the gel wax deeper in the cup (thermocouples 1 and 2). This resulted in a vertical thermal gradient, hence an inhomogeneous temperature distribution built up over time. After 50 minutes, the top part of the gel wax was insulated with a styrofoam disc, but the cooling rate of the top part of the gel wax (thermocouples 3 and 4) hardly changed.

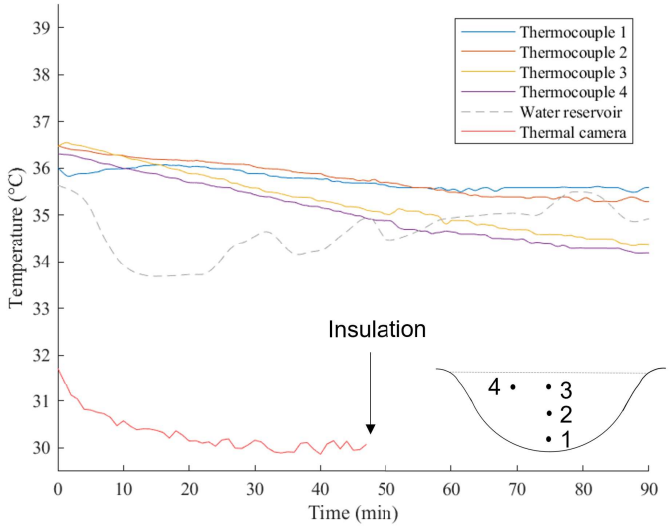

Figure 6.15: Temperature-time diagram from temperature inside the gel wax, when the water flow through the surface layer of the phantom was 36 °C. The temperature inside the gel wax was measured with four thermocouples at different positions, as indicated in the subplot. The gel wax surface temperature was measured with a thermal camera. After 50 minutes, the top layer of the phantom was insulated with styrofoam.

Experiment 4: Gel wax temperature stability with 25 °C water layer

During the first 6 minutes of the experiment, the temperature measurements indicate the presence of a negative vertical temperature gradient from thermocouple 2 to 3 in the upper half of the gel wax, see Figure 6.16. Such a gradient seemed absent between thermocouples 1 and 2 in the bottom half of the gel wax. Thermocouples 3 and 4 give no indication of a horizontal temperature gradient in the upper part of the gel wax.
After 6 minutes of cooling the gel wax with a flow of 25 °water, the gel wax temperature at the bottom of the phantom (thermocouple 1) started to drop, while the temperature at the other positions stayed constant. The observed cooling rate of the gel wax at the bottom was 0.1 °C/min.

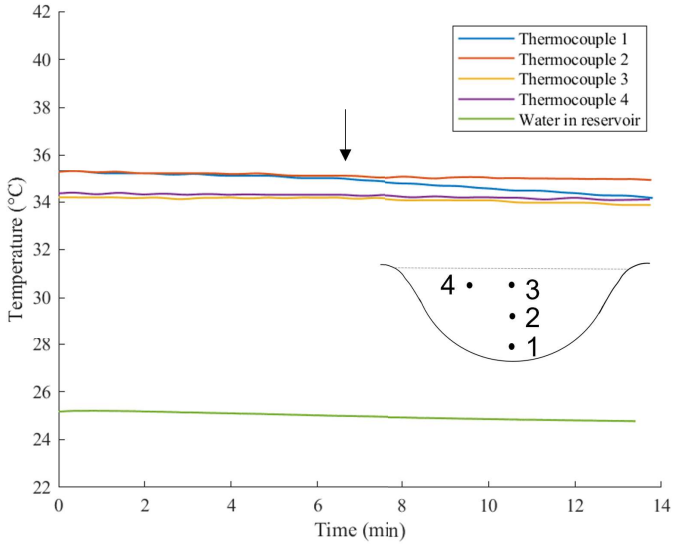

Figure 6.16: Temperature-time diagram from temperature inside the gel wax, when the water flow through the surface layer of the phantom was 25 °C. The temperature inside the gel wax was measured with four thermocouples at different positions, as indicated in the subplot. The arrow indicates the moment at which the temperature of the gel wax at the bottom of the phantom (thermocouple 1) starts to drop.

6.4 Discussion and conclusion

The results of the final phantom have shown that the modifications made, based on the results of the prototype phantom, were successful. Most importantly, the new design of the water supply ring ensured almost no air accumulated between the PVC cups. Only small air bubbles remained in the top part of the phantom, but this poses no problem because those bubbles are outside the field of view of the PAMMOTH imager.

The surface temperature of the phantom was shown to be inhomogeneous and not stable over time when a water flow was absent. With the presence of a warm water flow, the surface seems much more homogeneous, however the mean temperatures of the sampling areas in the periphery area were considerably lower. This can be explained by the so-called curvature effect. A temperature drop due to the curvature effect arises because the emissivity decreases as the angle between the viewing angle and the normal direction is larger than 60 °[38]. Considering only the central areas with minimal curvature effect, the temperature values do not differ significantly over the phantom's surface, and therefore the surface temperature can be considered homogeneous.

The phantom's water layer could be kept at constant temperature by the hot plate, but once placed inside the imaging bowl of the PAMMOTH (25 °C water) the temperature decreased by order 1-2 °C compared to the set temperature of the hot plate. The temperature feedback loop of the hot plate did not correct this drop, despite the set temperature was not met. A possible explanation is that the feedback loop is likely programmed to stop heating the liquid before the set temperature is reached to prevent an overshoot. The temperature (relative to set temperature) at which heating is programmed to stop, is likely optimized for the condition of heating a fluid without any inflow of a cooler fluid. In the case of the phantom in 25°C, a continuous inflow of slightly cooled water from the phantom enters the reservoir.

During experiment 3 (gel wax temperature stability and homogeneity), it was intended to match the temperature of the water layer with the temperature of the pre-heated gel wax, to avoid the formation of a temperature gradient inside the gel wax. However, this was not achieved due to the issues with the hot plate temperature feedback loop (see previous paragraph). Since the temperature of the gel wax was higher than the temperature in the water layer, heat was likely transferred from the gel wax to the water, resulting in cooling of the gel wax close to the water layer. The rate of cooling of the gel wax was higher at the top of the phantom (thermocouples 3 and 4) compared to the bottom. The gel wax at the top of the phantom likely loses its heat to the surrounding air, which is supported by the relatively low surface temperature measured with the thermal camera. This indicates that the heat loss of the gel wax at the top surface to the surrounding air was more prominent than the heat loss to the water layer. This stresses the need for good insulation of the gel wax top layer to improve the temperature stability and homogeneity of the gel wax part of the phantom.
Although cooling of the pre-heated gel wax is undesirable, the observed cooling rate was very low, such that over a 5-minute period (duration of a PAMMOTH measurement) the temperature may be considered constant. Therefore, the pre-heating procedure of the gel wax in a water bath has been shown to improve the stability and homogeneity of the gel wax, compared to the use of room temperature gel wax (Section 5.3.2). However, the pre-heating procedure still took hours 2.5 hours. To reduces this time, the temperature of the water bath could be increased, but a temperature overshoot should be avoided.

Experiment 4 mimicked the situation of putting pre-heated gel wax directly in contact with the water in the imaging bowl. Interestingly, the gel wax temperature remained constant at all thermocouple locations. Only after 6 minutes, the temperature of the gel wax close to the 25 °C water (thermocouple 1) started to drop. Since the temperature was stable for the duration of one PAMMOTH measurement, it raises the question whether pre-heated gel wax alone, without a heated surface water layer, could also be a suitable test object.

7 Photoacoustic reconstructions

7.1 PAMMOTH measurements

7.1.1 Materials and methods

Phantom setup

The final phantom setup used during the PAMMOTH measurements was the same as the previously described test setup in the lab (Section 5.2.1), except the phantom is now placed in the imaging bowl of the PAMMOTH. The water used to fill the imaging bowl was first degassed in an in-house setup with a gas-liquid separation membrane. The final setup of the phantom in the PAMMOTH is shown in Figure 7.1. The water reservoir was placed 30 cm below the surface of the PAMMOTH table and the pumping speed was set at 2.80 (arb. unit) to ensure equal water in- and outflow. Two thermocouples were included in the upper part of the gel wax at intermediate and centre position (see Figure 5.12) to monitor the temperature inside the gel wax during the measurements. The thermocouples were placed high to minimize the disturbing PA signal from the thermocouples. One thermocouple was placed in the water reservoir to monitor the temperature of the water that flowed through the outer layer of the phantom. These temperature measurements are required for the PA reconstructions, as will be explained later.

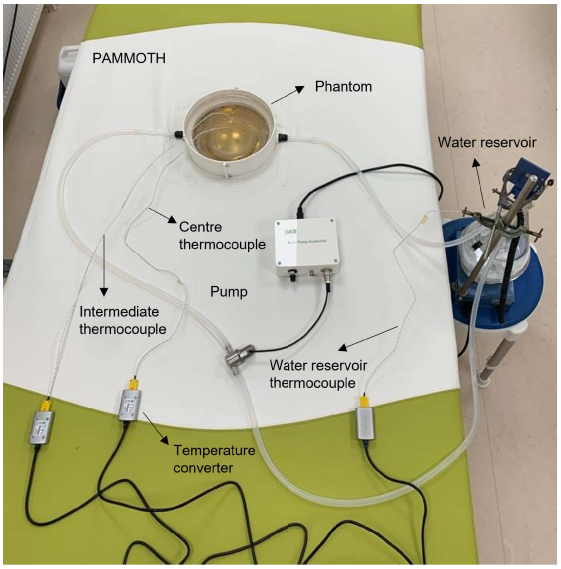

Figure 7.1: Image of the final phantom setup in the PAMMOTH imager at the MST hospital in Oldenzaal. The phantom is placed inside the imaging bowl and connected to a pump and a temperature controlled water reservoir. Two thermocouples are placed inside the gel wax of the phantom and one thermocouple is placed inside the water reservoir.

Measurement procedure

The patient protocol, described in the thesis of M. Dantuma *et al.* (Section 6.4.4.) [11] was used. This protocol was used such that the results of the PA reconstructions are translatable to reconstructions patient data. The photoacoustic measurement sequence consisted of a set of five PA excitation wavelengths being 720, 755, 797, 833, and 870 nm. For each wavelength, four excitation light pulses were sent per bowl position (4 averages). The bowl rotates around its central axis to acquire multiple projections. In each measurement, 101 bowl positions were used to cover 360 degrees. After each light pulse, all 512 US transducers are in detection mode. The repetition rate of the laser was 10 Hz and the repetition rate of the US emission was 100 Hz. This allows emission of nine US pulses in between two light pulses. The total acquisition time was 5 minutes per measurement.

Experiments

Before the first measurement, the phantom was pre-filled with degassed water and the closed-loop system was made. The water in the reservoir (3L Erlenmeyer) was heated to 25 °C on a hot plate magnetic stirrer (IKAMAG RET-G) with a temperature control sensor (IKA® IKATRON™ ETS-D4). To ensure homogeneous water temperature the magnetic stirrer was set to stir at 250 rpm. The gel wax had a temperature of 25.5 °C before the start of the experiment. This measurement with the 25 °C phantom was repeated twice.

The next measurements were conducted with the phantom at higher temperatures. Two measurements were conducted with the water in the reservoir at 33 °C, and one measurement was conducted with 35 °C water. These temperatures are in the range of body temperature, and were used because these were the temperatures at which the hot plate stabilized. Since these water temperatures are higher than the temperature of the gel wax, it was necessary to pre-heat the gel wax to ensure a stable temperature during the measurements. The gel wax was pre-heated in an external water bath of 50 °C for 1 hour and 45 minutes. After the heating procedure in the water bath, the top part of the phantom was isolated with styrofoam disc to prevent rapid cooling of the gel wax. The measurement was started when the temperature of the water in the reservoir stayed constant at 33 or 35 °C. During a measurement, the recirculation speed of the water in the imaging bowl was set at its lowest value to minimize disturbances (e.g. formation of air bubbles) and in between measurements the recirculation speed was set at its highest value for optimal cooling.

Table 7.1: Overview of the six experiments conducted in the PAMMOTH imager.

Measurement	Description
1	Phantom water temperature set at 25 °C, gel wax at room temperature
2	Phantom water temperature set at 25 °C, gel wax at room temperature
3	Phantom water temperature set at 33 °C, gel wax pre-heated
4	Phantom water temperature set at 33 °C, gel wax pre-heated
5	Phantom water temperature set at 35 °C, gel wax pre-heated

Photoacoustic reconstructions

The photoacoustic reconstructions were made for a single wavelength of 797 nm on a 0.4 mm grid (spatial resolution), and were based on a three-compartment SOS model (3-SOS model). The 3-SOS model assigned different speed of sound values to the water in the PAMMOTH imaging bowl, the water in the outer layer of the phantom and the gel wax in the phantom, see illustration in Figure 7.2. This model assumes that the outer cup (size 8) of the phantom is ideally positioned in the imaging bowl and that the water layer in the phantom has a thickness of 22 mm inwards from the surface of cup 8. The SOS of the water in the PAMMOTH imaging bowl is determined by first averaging the temperature measured by the two PT100 temperature sensors in the imaging bowl, followed by

a conversion to the corresponding SOS with Equation 2.3 (Section 2.4). The SOS of water in the outer layer of the phantom is determined by measuring the temperature of the water in the reservoir during a measurement and again using Equation 2.3. The SOS in the gel wax (c_{gw} in m/s) is determined by calculating the average measured temperature (T) for both thermocouples at centre and intermediate position separately, followed by a conversion to the SOS using a weighted least-squares (WLS) regression fit [32]:

$$c_{gw} = -4.4230 \cdot T + 1529.71, \tag{7.1}$$

This characterization of the temperature-dependent SOS of gel wax was done by Bakaric *et al.* [32] with a photoacoustic thermometry setup. The type of native gel wax used, was the same gel wax as used in the current study.

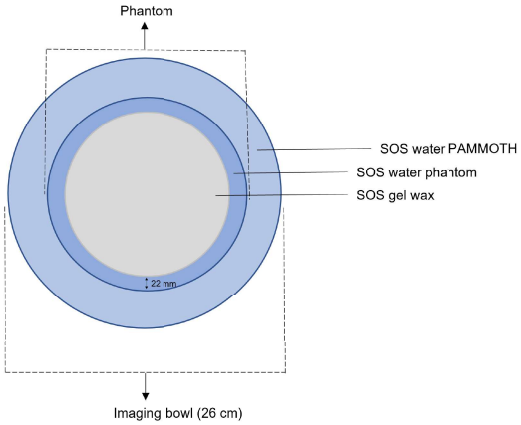

Figure 7.2: Schematic 2D drawing of the PAMMOTH imaging bowl with the phantom (top view) to illustrate the three different parts in the 3-SOS model.

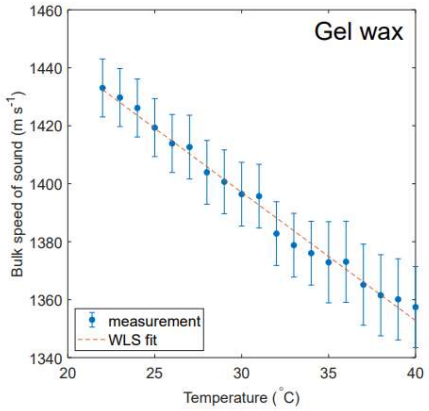

Figure 7.3: Measured SOS of gel wax as a function of temperature. The dotted line represents a weighted least-squares regression fit (Equation 7.1), were the weight was the inverse of the variance squared. The error bars represent the uncertainty (p=0.95), which ranges from 9-17% along the temperature range. Figure from [32].

7.1.2 Results

In this section, the results of measurement 1 and measurement 5 will be shown. Due to limited time, other measurements are not discussed.

Figure 7.4 show the maximum intensity projections (MIPs) of the PA measurement of the phantom along the x-, y-, and z-axis for measurement 1. The MIP shows that the PA targets inside the gel wax are generally reconstructed as clear dots. During this measurement, the temperature of the water in the reservoir, and thus in the water layer encapsulation the gel wax, remained constant at 25.8 °C for the longest part of the measurement, see Figure 7.5. Also, the temperature of the water in the imaging bowl hardly fluctuated (max. 0.1 °C). It is remarkable that the temperature of the gel wax, measured at both intermediate and centre position, increased after the start of the measurement and decreased again after the measurement. The gel wax temperature after the measurement was approximately similar to the temperature before the measurement.

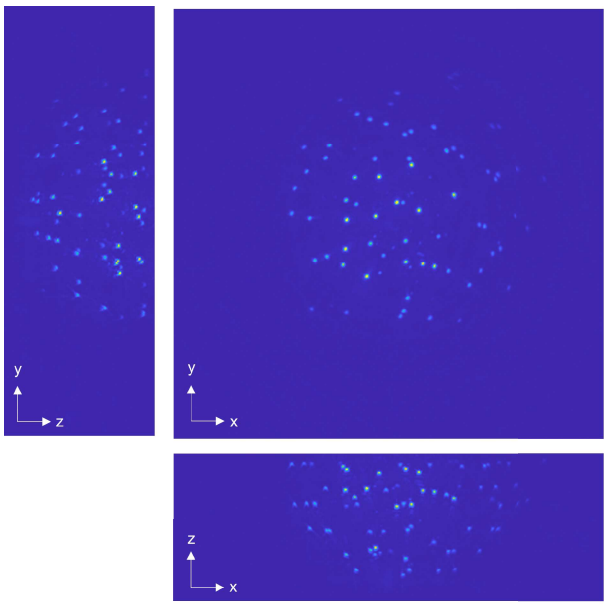

Figure 7.4: Maximum intensity projections (MIPs) of the PA reconstruction of the phantom along the x-, y- and z-axis for measurement 1 (25 °C phantom). The SOS values for the reconstructions were 1497 m/s, 1499 m/s and 1425.5 m/s for the water in the imaging bowl, water in the phantom and the gel wax respectively.

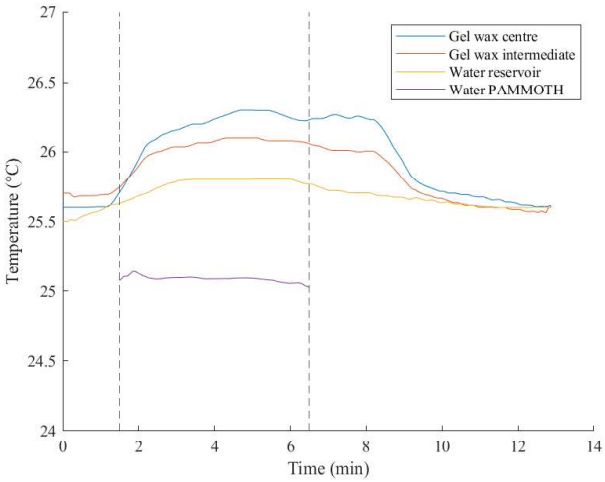

Figure 7.5: Temperatures measured during the PA measurement with the phantom at 25 °C. The dashed lines indicate the start and end of the PA measurement.

Figure 7.6 show the maximum intensity projections (MIPs) of the PA measurement of the phantom along the x-, y-, and z-axis for measurement 5. The MIP shows that the PA targets inside the gel wax are reconstructed as large blurred structures (yz- and xz-plane) and ring-shaped structures (xy-plane). The temperature measurements show that the water in the imaging bowl, the water in the phantom, and the gel wax stayed constant over the duration of the measurement, see Figure 7.7. However, it can be seen that the temperature of the gel wax was pre-heated to temperatures higher than the temperature in the reservoir. Moreover, the temperature at intermediate position was 0.5 °C lower than the temperature in the middle. Also during this measurement, the temperature of the gel wax increased and again decreased after the measurement.

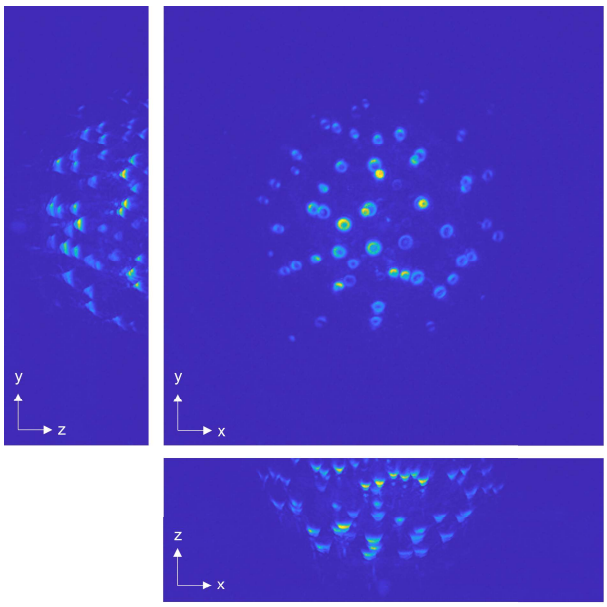

Figure 7.6: Maximum intensity projections (MIPs) of the PA reconstruction of the phantom along the x-, y- and z-axis for measurement 5 (35 °C phantom). The SOS values for the reconstructions were 1497.8 m/s, 1520.1 m/s and 1365 m/s for the water in the imaging bowl, water in the phantom and the gel wax respectively.

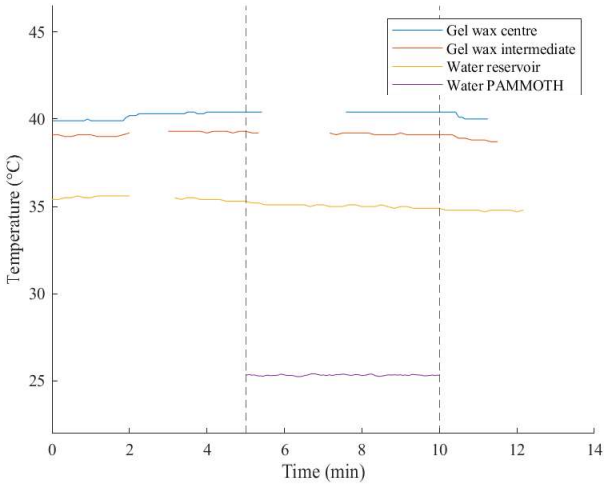

Figure 7.7: Temperatures measured during the PA measurement with the phantom's water layer at 35 °C. The dashed lines indicate the start and end of the PA measurement. Gaps in the data are due an error in the data logging device.

7.2 Discussion and conclusion

The temperature increase measured by the thermocouples in the gel wax was observed during all measurements (measurement 1-5). This can likely be explained as a result of heating by the lasers. The IR light could have been absorbed by the thermocouple wires, leading to a temperature increase measured by the thermocouples, rather than a real increase in gel wax temperature. However, the thermocouples were not inside the field of view, and therefore it was not possible to see whether the thermocouples indeed generate a photoacoustic signal.

It was shown that a good reconstruction could be made of the targets when the water in the reservoir and the temperature of the gel wax were both 25 °C. During this measurement, there was no temperature inside the gel wax measured, which is plausible because the gel wax temperature was equal to the temperature of the water in the water layer. Therefore, assigning only one SOS to the gel wax in the 3-SOS reconstruction model poses no problem. This was not the case in the measurements with the phantom at body temperatuur (33 and 35 °C). Since the pre-heating procedure in a 50 °water bath was not sufficiently controllable, the gel wax was heated to approximately 40 °C. This was considerably higher than the temperature of the water flowing through the outer layer of the phantom. Heat was likely transported from the gel wax water, which cause the formation of a temperature gradient inside the gel wax. Assigning only one SOS to the gel wax in the 3-SOS reconstruction model could have contributed to reconstruction artifacts observed. The reconstructions of measurement 5 are repeated with seven different SOS values ranging from 1365 to 1625 m/s, see Appendix G. A relatively good reconstruction was achieved for a SOS of 1405 m/s. Strangely, this SOS corresponds with a gel wax temperature of 28.2 °C, which is approximately 10 °C below the measured gel wax temperature. An explanation for this is currently still lacking. Speed of sound maps

could be useful to better explain the observed results. SOS-maps take into account inhomogeneities in SOS in the medium, and therefore in principle also inhomogeneities in temperature. It could be useful to use a SOS map for the reconstructions instead of a 3-SOS model, however first the validity of this SOS map should be investigated. An additional PA measurement was performed, in which the gel wax of the phantom was homogeneously heated to 36 °C, and the temperature of the water in the reservoir was matched to this. This measurement aimed to show if the reconstructions turned out better with a homogeneous and stable gel wax temperature because this was not the case in the first set of experiments. However, reconstructions of this measurement were not provided in time for this project.

8 Discussion

In this study, a temperature-controlled breast phantom was developed and its temperature stability was characterized. This chapter discusses to what extent the design met the set requirements and provides recommendations for further improvement of the design.

The developed phantom consisted of two main parts: a temperature control system, and a breast tissue mimicking part. In total twelve requirements were defined for these parts (Chapter 3). All requirements with an importance factor of 4 or 5 were met, except requirement V, XI and XII which were only partially met.

Requirement V states that the SOS value of the tissue mimicking material should be in the range relevant to breast tissue, namely 1430-1520 m/s [24]. At room temperature, the SOS of gel wax falls within this range (1441.2 m/s at 20 °C [32]). However, increasing the temperature of the gel wax results in a decrease in the SOS of the gel wax below the SOS range relevant to breast tissue [32]. This was already identified as a threat (Section 4.4), but by choosing for heating a water layer around the gel wax, initially the need for heating the gel wax itself was not foreseen. However, characterization experiments have shown that pre-heating gel wax was required to achieve a more stable temperature. This implies a trade-off had to be made between a stable SOS (stable temperature) or staying in the range of SOS values for breast tissue. Considering this phantom needs to be used for the aforementioned repeatability study, a stable SOS outweighs having a SOS in the range of breast tissue. Namely, if the phantom itself has an unstable SOS, it is not possible to investigate the effect of temperature fluctuations, hence SOS fluctuations, in the water in the imaging bowl.

Requirement XI states that the temperature of the phantom must be very stable and homogeneous. It was shown that with the flowing water layer around the phantom, a homogeneous surface temperature could be achieved. However, the current temperature system has shown to lack the ability to quickly compensate for the heat loss from the phantom to the water in the imaging bowl. The water temperature stabilizes after approximately 10 minutes, but at an unpredictable value. This is undesirable for a repeatability study, in which full control over the phantom's temperature is important to make sure that in every repeated measurement the test object is the same. On the positive side, the temperature in the water layer remained very constant over the duration of a PAMMOTH measurement (5 minutes), independent of the set temperature.

Considering the gel wax part of the phantom, it was found that pre-heating is required to maintain a stable temperature inside the gel wax, provided that the temperature in the water layer matches the gel wax temperature. Getting the gel wax homogeneously pre-heated to a defined temperature was achieved, but was time consuming (typically 3 hours). It was more difficult to maintain the temperature of the gel wax stable and homogeneous, mainly due to cooling of the top surface of the gel wax (not insulated). However, this cooling rate was very low and

therefore the gel wax temperature could be considered constant over the duration of a PAMMOTH measurement. More problematic is the appearance of a spatial temperature gradient over time, which decreases the applicability of a 3-SOS model for PA reconstructions. Provided the temperature inhomogeneity is stable over the time span of a PAMMOTH measurement, the expectation is that SOS maps may be able to take into account the temperature induced SOS inhomogeneities for PA reconstructions. Therefore, to completely fulfill requirement XI, some further improvements are needed for water temperature control and for insulation on top of the phantom.

Requirement XII states that the temperature inside the phantom should be known, by monitoring the temperature inside the gel wax as well as the temperature of the water flowing through the phantom's outer layer. In this study, thermocouples were used to monitor the temperature at different positions inside the phantom. With this type of temperature sensors, it was possible to quantitatively describe warming and cooling rates of the phantom at individual sensor locations, and therefore characterize the temperature stability over time. However, it was not possible to quantitatively describe the spatial temperature gradients resulting from spatially varying cooling or warming trends. This is because some of the temperature differences are in the same order of magnitude as the temperature sensor accuracy. In Section 6.3, it was described that a calibration was needed to compensate for a varying accuracy of the cold junction compensation sensor (typically 0.6 °C, max. 1.25 °C) inside the converter. Additionally, errors in temperature measurements also depend on the accuracy of the thermocouple itself and is typically ± 2.2 °C or 0.75% (which ever is greater) for K-type thermocouples [39]. Requirement XII is only partially met because the temperature inside the phantom was known, but with relatively low accuracy. For this study, the temperature should be known with a higher accuracy, because relatively large inaccuracy in the measured temperatures leads to relatively large inaccuracy in the calculated SOS values inside the phantom, which eventually could have contributed to low quality PA reconstructions.

Recommendations

- In the current study a trade-off had to be made between a stable SOS (stable temperature) or staying in the range of SOS values relevant to breast tissue. Gel wax has many advantageous properties, but the decreasing speed of sound with temperature is a drawback [32]. The tunability of the SOS of gel wax is limited because additives to increase the SOS also result in high acoustic attenuation. A possible option to overcome this limitation, is the use of another material. A possible substitute for gel wax could be a copolymer-in-oil formulation [40]. This is a tissue-mimicking material consisting of mineral oil, copolymer and stabilizers. Most properties are comparable to gel wax, but the acoustic properties could be tuned up to 1516 ± 0.6 m/s while keeping the acoustic attenuation relevant to soft tissue. This speed of sound is in the higher end of the range relevant to breast tissue, and therefore a possible decrease in SOS due to a temperature increase is allowed. The exact temperature-dependent speed of sound of copolymer in oil still needs to be investigated to confirm if the SOS in the range of body temperature indeed falls within the range relevant to breast tissue.
- To improve the stability of the temperature of the water in the outer layer of the phantom, it is recommended to use another heating system than a hot plate. Both hot plates used in study were incapable of keeping the water at the desired set temperature. An alternative heating system that could be used is a precision cooker. Precision cookers can be placed in a water bath to heat the water to a precise temperature. Moreover, the water is circulated which ensures a homogeneous temperature. The precision cooker was already used in this study for thermocouple calibration and showed that the water could be quickly heated to a desired set

temperature and even more important, is able to quickly compensate for a drop in the water temperature. Moreover, the precision cooker can heat larger volumes of water than a hot plate and which makes it less sensitive to the inflow of slightly cooled water from the phantom.

- The first PAMMOTH results require further analysis, including possible improvements to be expected from using a SOS-map in the PA reconstruction. For validation of the SOS-map, a more detailed characterization of the temperature distribution inside the gel wax is needed. To achieve this, fiber optic temperature sensors could potentially be a good alternative to the thermocouples used in this study. These sensors can collect temperature measurements at multiple location along a fiber [41], with an accuracy of around 0.2 °C and a resolution smaller than 0.1 °C [42]. Temperature measurement along the fiber can have mm-scale spatial resolution [41]. By using multiple fibers in the phantom's gel wax, a temperature map could be made. This map can than be compared to the SOS-map obtained in a PAMMOTH measurement, to asses its validity for using it in PA reconstructions.

9 Conclusion

The objective of this study was to design and develop a temperature-controlled breast phantom that is suitable as a test object for the investigation into the temperature fluctuations in the water of the PAMMOTH imaging bowl. For this, first a set of twelve requirements was made. Following the phases of concept design, prototype design, and final design, a test object was fabricated, characterized, and verified. The test object was subsequently used in the PAMMOTH system to demonstrate the importance of developing such an object as well as to test the feasibility of using the object in the intended environment as envisaged.

The formulated requirements were mainly based on considerations regarding the stability of the test object, required for repeated measurements, and the suitability for being used in a PA tomographic breast imaging system.

The developed phantom consisted of two main parts: a breast tissue-mimicking part and a temperature-regulating system. The temperature system consisted of a water flow circuit consisting of a water supply ring in between two breast shaped cups. The water supply ring was connected to a closed-loop pumping system and a water reservoir that was heated by a hot plate. The tissue-mimicking part was placed inside the inner cup and consisted of gel wax in which subresolution PA targets were embedded.

The temperature stability and homogeneity of the phantom was tested with regard to the water layer around the phantom and the gel wax part inside the phantom. The water layer had of the phantom a homogeneous temperature distribution and stayed stable over the duration of a PAMMOTH measurement. However, due to shortcomings of the hot plate, there was limited control over the exact temperature at which it stabilized. The temperature of the gel wax was shown to slowly cool down but at a very low rate such that it could be considered stable over the duration of a PAMMOTH measurement. This conclusion applies only if the gel wax was pre-heated to the same temperature as the water flowing through the water layer.

These findings imply that the developed phantom in its current state is not yet ready to be used as a test object in a repeatability study, as the temperature of the test object cannot be ensured to have exactly the same temperature in each repeated measurement. However, it is expected that improvements of the heating source for heating the water and better insulation of the gel wax can improve the stability of the phantom, thereby making it suitable for repeated measurements.

Acknowledgements

During my thesis project I received much appreciated help and input from various people. Firstly, I want to thank my daily supervisor Rianne Bulthuis for her enthusiasm in thinking along with me, providing feedback and helping me with the experiments in the PAMMOTH system in the hospital of Oldenzaal. Further, the phantom could not have been fabricated without the help of Johan van Hespen. Besides assisting and thinking along in the actual production of the phantom, he implemented the designs for the water circuit ring and the custom size cup mold in SolidWorks and realized the 3D printing of these elements. Next, I kindly want to acknowledge prof. dr. Srirang Manohar, chair of my thesis committee, for his enthusiasm and input in my thesis project, as well as for giving me the opportunity to be part of the M3I group and the PAMMOTH project. In the lab, I received highly appreciated help from Jitse Giesen. I want to thank him for his helping me with the thermal camera measurements and his enthusiasm in thinking along with me on several topics. In addition, Maura Dantuma kindly helped me with coating the photoacoustic targets. Tom Knop is greatly acknowledged for letting me borrow his thermal camera, that made it possible to evaluate temperature homogeneity along the phantom's surface. I also want to thank Felix Lucka for making the photoacoustic reconstructions of the phantom. Finally, the M3I people are warmly thanked for making me feel welcome in the group.

References

[1] World Health Organization. *Breast cancer*. 26 March 2021. https://www.who.int/news-room/fact-sheets/detail/breast-cancer (accessed May 1, 2022).

[2] Hyuna Sung et al. "Global Cancer Statistics 2020: GLOBOCAN Estimates of Incidence and Mortality Worldwide for 36 Cancers in 185 Countries". In: *CA: A Cancer Journal for Clinicians* (2021;71:209-249). doi: 10.3322/CAAC.21660.

[3] Steven A. Narod, Javaid Iqbal, and Anthony B. Miller. "Why have breast cancer mortality rates declined?" In: *Journal of Cancer Policy* (2015;5:8-17). doi: 10.1016/J.JCPO.2015.03.002.

[4] Archie Bleyer and H. Gilbert Welch. "Effect of Three Decades of Screening Mammography on Breast-Cancer Incidence". In: *New England Journal of Medicine* (2012;367:1998-2005). doi: 10.1056/nejmoa1206809.

[5] National Cancer Institute (n.d.) *Definition of adjuvant therapy - NCI Dictionary of Cancer Terms*. Visited on: June 6, 2022. URL: `https://www.cancer.gov/publications/dictionaries/cancer-terms/def/adjuvant-therapy`.

[6] Mariko Asaoka et al. "Neoadjuvant Chemotherapy for Breast Cancer: Past, Present, and Future". In: *Breast Cancer : Basic and Clinical Research* (2020;14). doi: 10.1177/1178223420980377.

[7] Li Lin et al. "Photoacoustic Computed Tomography of Breast Cancer in Response to Neoadjuvant Chemotherapy". In: *Advanced Science* (2021:8;2003396). doi: 10.1002/ADVS.202003396.

[8] Jamal Majidpoor and Keywan Mortezaee. "Angiogenesis as a hallmark of solid tumors - clinical perspectives". In: *Cellular oncology (Dordrecht)* (2021;44:715–737). doi: 10.1007/S13402-021-00602-3.

[9] Keerthi S. Valluru and Juergen K. Willmann. "Clinical photoacoustic imaging of cancer". In: *Ultrasonography* (2016;35:267). doi: 10.14366/USG.16035.

[10] Paul Beard. "Biomedical photoacoustic imaging". In: *Interface Focus* (2011;1:602). doi: 10.1098/RSFS.2011.0028.

[11] Maura Dantuma. *A hybrid multispectral photoacoustic-ultrasound breast image from the lab towards the clinic*. isbn: 978-90-365-304-9, doi: 10.3990/1.9789036553049. 2021, pp. 127–158.

[12] Gladis A.parecida Galindo R.eisemberger de Souza et al. "Reference breast temperature: proposal of an equation". In: *Einstein* (2015;14:518). doi: 10.1590/S1679-45082015AO3392.

[13] Dominique van de Sompel et al. "Improving image quality by accounting for changes in water temperature during a photoacoustic tomography scan". In: *PloS one* (2012;7). doi: 10.1371/JOURNAL.PONE.0045337.

[14] Ganesh N. Sharma et al. "VARIOUS TYPES AND MANAGEMENT OF BREAST CANCER: AN OVERVIEW". In: *Journal of Advanced Pharmaceutical Technology & Research* (2010;1:109). issn: 01105558.

[15] Yixiao Feng et al. "Breast cancer development and progression: Risk factors, cancer stem cells, signaling pathways, genomics, and molecular pathogenesis". In: *Genes & Diseases* (2018;5:77-106). doi: 10.1016/J.GENDIS.2018.05.00

[16] Keerthi S. Valluru and Juergen K. Willmann. "Clinical photoacoustic imaging of cancer". In: *Ultrasonography* (2016;35:267). doi: 10.14366/USG.16035.

[17] Jun Xia, Junjie Yao, and Lihong V. Wang. "Photoacoustic tomography: principles and advances". In: *Electromagnetic waves (Camb)* (2014;147:1). doi: 10.2528/PIER14032303.

[18] Si Wu and Hans Jürgen Butt. "Near-infrared photochemistry at interfaces based on upconverting nanoparticles". In: *Physical Chemistry Chemical Physics* (2017;19:23585-23596). doi: 10.1039/C7CP01838J.

[19] Tianrui Zhao et al. “Minimally invasive photoacoustic imaging: Current status and future perspectives”. In: *Photoacoustics* (2019;16:100-146). doi: 10.1016/J.PACS.2019.100146.

[20] Chao Tian et al. “Spatial resolution in photoacoustic computed tomography”. In: *Reports on progress in physics. Physical Society (Great Britain)* (2021;84). doi: 10.1088/1361-6633/ABDAB9.

[21] Sjoukje M. Schoustra et al. “Pendant breast immobilization and positioning in photoacoustic tomographic imaging”. In: *Photoacoustics* (2021;21:100238). doi: 10.1016/J.PACS.2020.100238.

[22] V. A. Del Grosso and C. W. Mader. “Speed of Sound in Pure Water”. In: *The Journal of the Acoustical Society of America* (2005;52:1442). doi: 10.1121/1.1913258.

[23] Shih Ying Huang et al. “The characterization of breast anatomical metrics using dedicated breast CT”. In: *Medical Physics* (2011;38:2180). doi: 10.1118/1.3567147.

[24] William C. Vogt et al. “Biologically relevant photoacoustic imaging phantoms with tunable optical and acoustic properties”. In: *Journal of Biomedical Optics* (2016;21:101405). doi: 10.1117/1.JBO.21.10.101405.

[25] Clarence Kemper and Göran Bringert. “Temperature measurement”. In: *Validation of Pharmaceutical Processes, Third Edition* (2021:423-468). doi: 10.1016/B978-0-12-817141-7.00014-1.

[26] Paulo Roriz et al. “Optical Fiber Temperature Sensors and Their Biomedical Applications”. In: *Sensors 2020, Vol. 20, Page 2113* (2020;4:2113). doi: 10.3390/S20072113.

[27] Sarah E. Bohndiek et al. “Development and Application of Stable Phantoms for the Evaluation of Photoacoustic Imaging Instruments”. In: *PLoS ONE* (2013;8:75533). doi: 10.1371/JOURNAL.PONE.0075533.

[28] Martin O. Culjat et al. “A Review of Tissue Substitutes for Ultrasound Imaging”. In: *Ultrasound in Medicine & Biology* (2010;36:861-873). doi: 10.1016/J.ULTRASMEDBIO.2010.02.012.

[29] Brian W. Pogue and Michael S. Patterson. “Review of tissue simulating phantoms for optical spectroscopy, imaging and dosimetry”. In: *Journal of Biomedical Optics* (2006;11:041102). doi: 10.1117/1.2335429.

[30] Bradley E. Treeby et al. “Automatic sound speed selection in photoacoustic image reconstruction using an autofocus approach”. In: *Journal of Biomedical Optics* (2011;16:090501). doi: 10.1117/1.3619139.

[31] Efthymios Maneas et al. “Gel wax-based tissue-mimicking phantoms for multispectral photoacoustic imaging”. In: *Biomedical Optics Express, Vol. 9, Issue 3, pp. 1151-1163* (2018;9:1151-1163). doi:10.1364/BOE.9.001151.

[32] Marina Bakaric et al. “Measurement of the temperature-dependent speed of sound and change in Grüneisen parameter of tissue-mimicking materials”. In: *IEEE International Ultrasonics Symposium, IUS* (2019;1-4). doi: 10.1109/ULTSYM.2019.8925838.

[33] Paola Di Ninni, Fabrizio Martelli, and Giovanni Zaccanti. “The use of India ink in tissue-simulating phantoms”. In: *Optics express* (2010;18:26854). doi: 10.1364/OE.18.026854.

[34] Sjoukje M. Schoustra et al. “Twente Photoacoustic Mammoscope 2: system overview and three-dimensional vascular network images in healthy breasts”. In: *Journal of Biomedical Optics* (2019;24:1). doi: 10.1117/1.JBO.24.12.121

[35] Ali Hariri et al. “The characterization of an economic and portable LED-based photoacoustic imaging system to facilitate molecular imaging”. In: *Photoacoustics* (2018;9:10-20). doi: 10.1016/J.PACS.2017.11.001.

[36] Jithin Jose et al. “Speed-of-sound compensated photoacoustic tomography for accurate imaging”. In: *Medical physics* (2012;39:7262-7271). doi: 10.1118/1.4764911.

[37] Paolo Scardina and Marc Edwards. “The Fundamentals of Bubble Formation in Water Treatment”. In: *Bubble Nucleation (Chapter 1)* (2009;2000:1-22).

[38] Tze Yuan Cheng, Daxiang Deng, and Cila Herman. "Curvature effect quatification for in-vivo IR thermography". In: *International Mechanical Engineering Congress and Exposition* (2012;2:127-133). doi: 10.1115/IMECE2012-88105.

[39] *USB-TC01 Specifications - NI*. Last update: 2022-05-03, (Accessed: 06-07-2022). URL: https://www.ni.com/docs/en-US/bundle/usb-tc01-specs/page/specs.html.

[40] Lina Hacker et al. "A Copolymer-in-Oil Tissue-Mimicking Material with Tuneable Acoustic and Optical Characteristics for Photoacoustic Imaging Phantoms". In: *IEEE Transactions on Medical Imaging* (2021;40:3593-3603). DOI: doi:10.1109/TMI.2021.3090857.

[41] Zhannat Ashikbayeva et al. "Distributed 2D temperature sensing during nanoparticles assisted laser ablation by means of high-scattering fiber sensors." In: *Scientific Reports* (2020;10:12593-12593). doi: 10.1038/S41598-020-69384-2.

[42] Sandra Drusová et al. "Comparison of three types of fiber optic sensors for temperature monitoring in a groundwater flow simulator". In: *Sensors and actuators. A: Physical* (2021;331:112682). doi: 10.1016/J.SNA.2021.112682.

Appendices

Cup mould and vacuum shaping PVC cups

A

In this Appendix additional information about the cup mould, and the vacuum shaping procedure of the PVC cups, can be found.

A.1 ABS cup mould

The cup mould was made from 3D printed (Ultimaker S5, The Netherlands) Acrylonitrile butadiene styrene (ABS). The resulting cup mould for the inner PVC cups is shown in Figure A.1A. The surface of the 3D printed cup mould had a ribbed structure due to the set layer thickness of the 3D printer. The surface of the cup mould needed to be smoother, otherwise the ribbed structure would also be visible in the PVC cup. Smoothing the cup mould was done by grinding with sandpaper (grid 180). The result is shown in Figure A.1B.

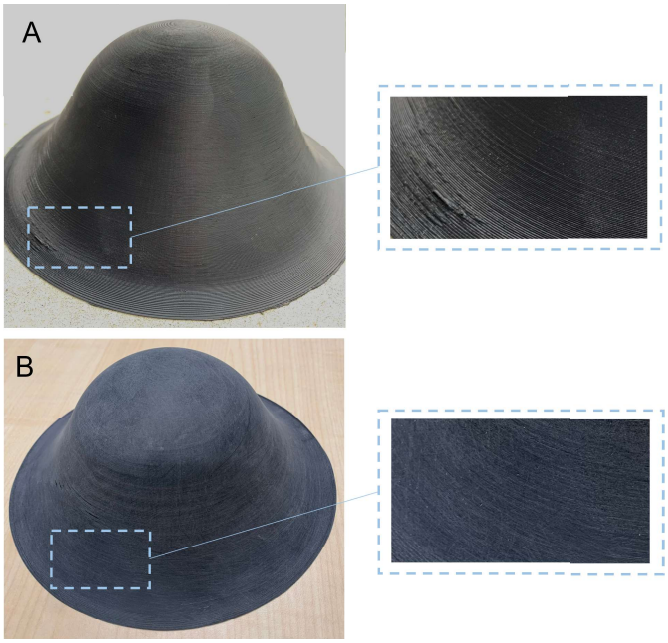

Figure A.1: ***A****: 3D printed ABS cup mould for vacuum shaping the inner PVC cup. The surface has a ribbed structure due to the set layer thickness.* ***B****: ABS cup mould after grinding with sand paper. The ribbed structure is diminished and the surface is smoother.*

A.2 Protocol 1: Vacuum shaping PVC cups

Materials

- PVC sheet (thickness 180 μm)
- Vacuum shaping machine (PA imaging)
- Cup mould size 8 (standard size)
- 3D printed cup mould from ABS (customized size and shape)

Vacuum shaping PVC cups

1. Place the size 8 cup mould in the vacuum shaping machine, see Figure A.2.
2. Cut a piece of PVC sheet and place it on the square frame above above the cup mould.
3. Turn on the heater of the vacuum shaping machine and let the PVC sheet heat for approximately 30 seconds.
4. Use the handle to press down the PVC sheet onto the cup mould. Turn on the vacuum pump and wait until all air is removed between the PVC sheet and the cup mould.
5. Remove the vacuum shaped PVC sheet from the mould and repeat step 1-4 for the customized cup mould.

Figure A.2: Cup mould (size 8) placed in the vacuum shaping machine at PA imaging.

Protocol 2: Coating microspheres with India ink

B

Materials

- Stainless steel microspheres (Coshperic LLC), diameter: 360-445 μm.
- India Ink (Thalens Indian ink Bottle 490 ml Black 700, article number: 44727000)
- Micropipette (Eppendorf Research Plus Adjustable Volume, Single Channel Pipette, 20 - 200 uL)
- Spatula
- Tweezers
- Petri dish (2x)
- PARAFILM (Sigma-Aldrich, article number: P7793)

Coating microspheres with India ink[1]

1. Pipette 1 droplet (100-200 μL) of India ink in the Petri dish.
2. Distribute $\pm$150 stainless steel microspheres in the droplet of ink and mix with a spatula until all microspheres are completely covered in ink. The microspheres tend to coagulate in the ink (see Figure B.1), therefore try to separate them with a spatula as well as possible.
3. Let the ink dry for 2-3 minutes.
4. Use tweezers or a spatula to take the microspheres out of the ink one by one, and place them on a piece of PARAFILM.
5. Place the coated microspheres in a clean Petri dish and close it with a piece of PARAFILM. The coated microspheres are now ready to be included in photoacoustic phantoms, see Figure B.2.

[1]Protocol developed by M. dantuma (pers. comm.) as applied in [11].

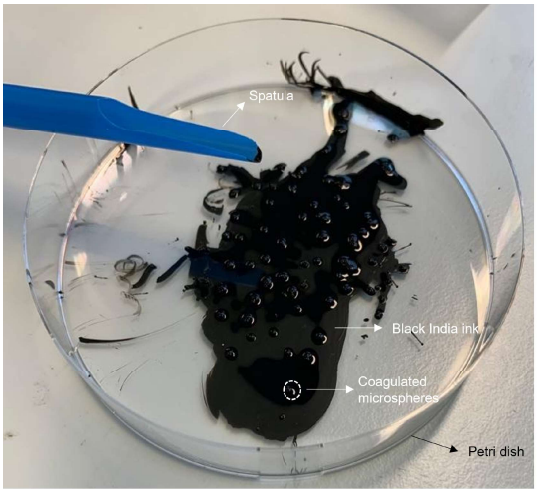

Figure B.1: The coating process of stainless steal microspheres with India ink inside a Petri dish. The microspheres are coagulated in the ink.

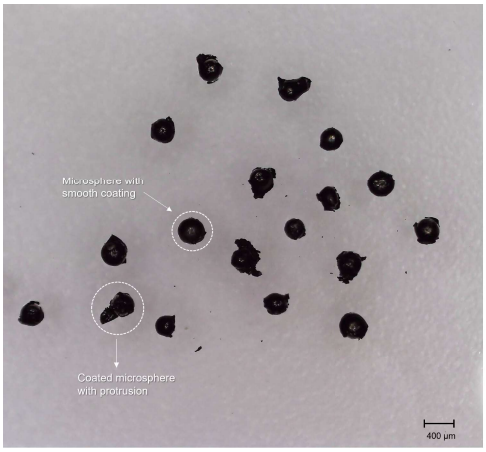

Figure B.2: Stainless steel microspheres after coating with India ink. The ink completely covers the surfaces of the microspheres, but sometimes exhibits irregular protrusions. Picture made with a tabletop microscope (RS PRO USB Digital Microscope, RS Stock No.: 196-4075).

Protocol 3: Gel wax casting

C

Materials

- Basic personal safety equipment (lab coat, gloves and glasses)
- Fume hood
- 2 kg of Native gel wax (Product number: FF1 003, Mindsets Online, Waltham Cross, UK)
- Digital weight scale
- Oil bath (IKA HB4 basic)
- Stand and clamps
- Vacuum oven (Heraeus)
- Heat-resistant gloves
- Metal spatula or spoon
- Glass beakers (2000 mL)
- Erlenmeyer flask (1000 mL)
- Glass funnel
- Phantom mould for casting (inner PVC cup glued to PLA ring)
- Round bowl (diameter 21-25 cm) filled with ice water
- Timer or clock
- Marker or pen
- Tape
- 130 stainless steel microspheres coated with India ink

Native gel wax preparation[1]

1. Turn on the oil bath at 150 °C to preheat. The temperature to which the oil bath is heated can be regulated on the oil bath itself. Also turn on the fume hood that the oil bath is in.

2. Turn on the vacuum oven at 100 °C to preheat.

3. Weigh 1 kg of native gel wax, divide it into several smaller pieces, and put in a 2000 mL glass beaker. (note[2]: 1 kg gel wax is enough to fill up the PVC cup, but additional gel wax is needed for the extra layer on top of the PVC cups. This will be elaborated later.)

4. Place the beaker with the gel wax in a clamp and secure it to a stand. Place the stand such that the part of the beaker that is filled hangs in the hot oil of the oil bath (see Figure C.1). Once the gel wax starts to melt. Stir with a metal spatula or spoon to help the melting process. Let the gel wax melt until it is fully liquid. Dependent on the amount that is used, this can take from several minutes to half an hour.

Figure C.1: The 2000 mL glass beaker is filled with native gel wax and placed in the oil bath of 150 °C. The gel wax inside the glass beaker was melted under regularly stirring with a metal spoon.

5. Once the solution is liquid, place it into the preheated vacuum oven. Turn on the vacuum pump and leave it on until all air bubbles have disappeared. This will take approximately 70 minutes. Then, release the vacuum by slowly turning the knob to let air into the oven. When the vacuum is released, take the beaker out of the vacuum oven. The solution is now ready to be poured into a mould.

[1] The first part of this protocol (native gel wax preparation) is modified after M. Krommendijk (BSc Thesis) [ref].

[2] The density of native gel wax is 0.850 g/mL [32]. The amount of gel wax needed to fill the inner PVC cup is 1 L and this is equal to **850 g**. The amount of gel wax needed to fill the part above the cup depends on the thickness of the layer. The required volume can be calculated with: $V = \pi \cdot r^2 \cdot h$. The diameter of the ring is 25 cm, therefore the radium (r) equals 12.5 cm. In this case the thickness of the gel wax layer is chosen to be 2.5 cm, therefore the required volume of gel wax is: $V = \pi \cdot 12.5^2 \cdot 2.5 = 1472 cm^3 = 1472 mL \approx$ **1000 g**. Thus, the total required mass of gel wax for the breast phantom is **1850 g**. Approximately 10 % extra gel wax was used to account for some loss of gel wax during the casting procedure.

Casting the gel wax

1. Place a piece of tape on the outside of the PVC cup from the bottom to the top and add marks on it to indicate layers of equal thickness[3], see Figure C.2. For this phantom, the cup has been marked for creating eight gel wax layers of 1 cm thickness each.

Figure C.2: Example of a PVC cup (top view) with marked tape to indicate the desired layer thickness. Example shown is a test version and not the final version used in the experiments.

2. Glue the inner PVC cup to the PLA ring with PVC glue. The inner PVC cup together with the PLA ring forms the mould for the gel wax.

3. Place the mould in a bowl filled with ice water. Cooling the mould prevents that the heated gel wax (T > 100 °C) melts or deforms the mould.

4. Pour the first layer of gel wax in the mould with a layer thickness of 1 cm, as indicated by the marks on the tape. Use a glass funnel to pour the gel wax carefully in the mould to prevent formation of new air bubbles. Let the layer solidify for approximately 1.5 - 2 minutes. Meanwhile, place the glass beaker with gel wax back in the oven to keep it melted.

5. When the surface of the gel wax layer has solidified, the photoacoustic targets (stainless steel microspheres coated with India ink) can be distributed over the layer. The number of targets per layer is listed in Table C.1[4]. Make sure the targets are evenly distributed over the surface with a minimum spacing of 1 cm, see Figure C.3.

Table C.1: Number of photoacoustic targets per layer of gel wax. Total number of targets is 127.

	Number of PA targets
Layer 1 (bottom)	5
Layer 2	8
Layer 3	10
Layer 4	12
Layer 5	15
Layer 6	20
Layer 7	24
Layer 8 (top)	33

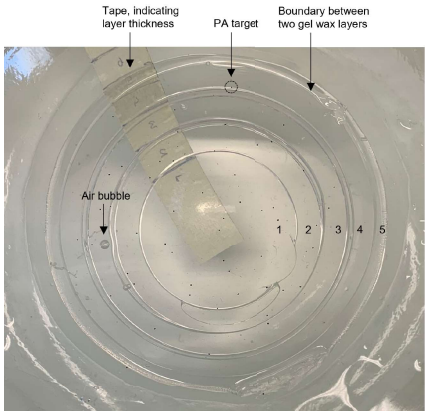

Figure C.3: Top view of PVC cup filled with 5 gel wax layers with PA targets evenly distributed over the surface of each layer.

6. Let the layer of gel wax solidify further for approximately 10 minutes. The next layer of gel wax can be poured on top of the previous layer. Step 4 and 5 must be repeated eight times until the PVC cup is completely filled with gel wax.

7. Melt the remaining 1 kg of gel wax by following steps 3 and 4 of the native gel wax preparation. This gel wax is used as an extra layer on top of the gel wax in the PVC cup. This layer is outside of the field of view of the PAMMOTH system and therefore it is not required to degas this gel wax in the vacuum oven.

8. Slowly pour all the melted gel wax in the mould. This extra gel wax layer does not have to be casted layer-by-layer.

9. Let the filled mould cool at room temperature until the gel wax has fully set. This might take several hours, dependent on the size of the phantom.

[3] The desired thickness of a layer (1 cm) is determined by filling the cup 'layer-by-layer' with water. The depth of the water is measured from the bottom of the cup to the surface of the water with a caliper. When the water has reached a height of 1 cm, a horizontal line was drawn on the tape at water level. This process was repeated every centimetre up until 8 cm. This completes the scale bar required for later filling the cup with equal layers of gel wax.

[4] The number of targets per layer is chosen such that the density of targets is approximately equal for all layers. An initial estimate of the required number of targets per layer was based on the total number of available targets and the surface area per layer.

Figure C.4 shows a microscope image of a coated microsphere inside the gel wax.

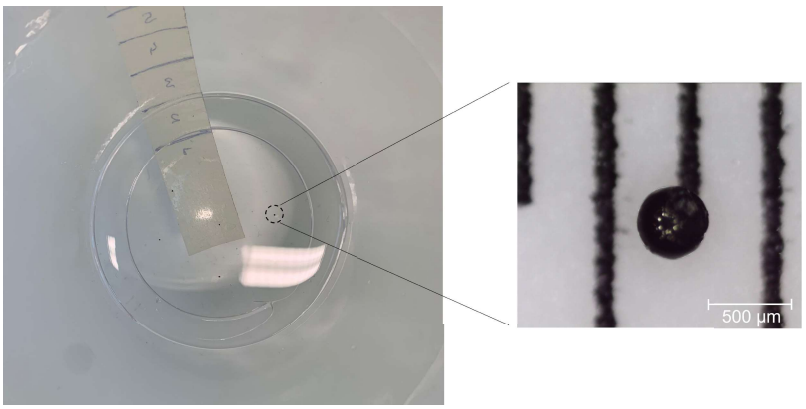

Figure C.4: Left: top view of inner PVC cup filled with the first two layers of gel wax with the India ink coated stainless steel microspheres distributed over the surface. Right: microscope image of stainless steel microsphere after manually coating with India ink. Picture made with a tabletop microscope (RS PRO USB Digital Microscope)

Additional Characterization results

D

D.1 Gel wax pre-heating procedure

The gel wax part of the phantom should be pre-heated to the same temperature as the water in the water circuit, otherwise a temperature gradient arises inside the gel wax.

Method

The prototype phantom was pre-heated in a 40 °C water bath. The phantom was entirely submerged in the water such that also the top part of the gel wax was in contact with warm water, instead of only the part inside the PVC cup.The temperature inside the gel wax was only monitored at intermediate and centre position (see Figure 5.12, since the gel wax close to the PVC cup first reaches a stable temperature, as shown in the results in Section 5.3.2. The temperature was logged with 1 Hz. The water in the water bath was maintained at 40 °by regularly replacing cooled water with new 40 °C water. The phantom was pre-heated until a stable and homogeneous gel wax temperature was reached.

Results

The temperature-time diagram is shown in Figure D.1. The gel wax at the intermediate position stabilized at 37 °C after 70 minutes. The gel wax at the centre position stabilized at 37 °C after 125 minutes. Since the temperature measured by both thermocouples stabilized at 37 °C, this suggest the temperature distribution inside the gel wax is quite homogeneous.

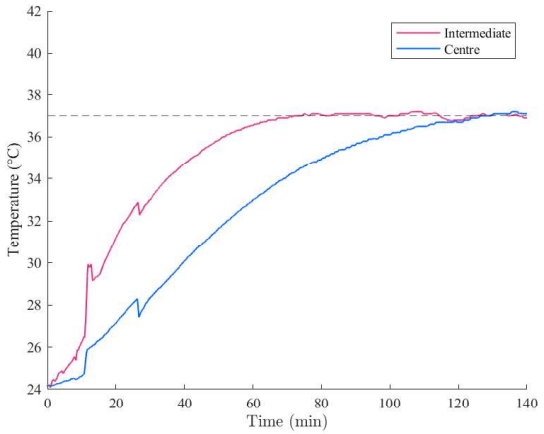

Figure D.1: Temperature-time diagram from the pre-heating procedure of the gel wax in a 40 °C water bath. The temperature inside the gel wax is measured with thermocouples at the centre and at intermediate position (indicated in Figure 5.12). The dashed line indicates a temperature of 37 °C.

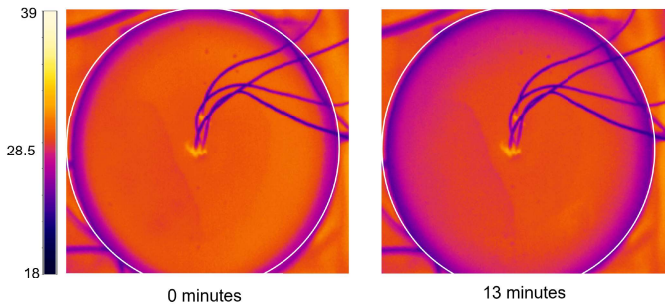

Figure D.2: Thermal camera image of the top part of the phantom, during experiment 4 (25° C water flow).

Thermocouple calibration

E

It is required to calibrate the thermocouples before use, such that every thermocouple gives an accurate temperature output. In the experiments, K-type thermocouples (XTVTX, EAN: 0768497313583) consisting of chromel/alumel and a white fiberglass insulation were used. The voltage generated by a K-type thermocouples is reasonably linear, staying near 41 μV/°C for temperatures above 0 °C. The thermocouples were connected to digital voltage-temperature converters (USB-TC01, National instruments). The cold-junction compensation accuracy is typically 0.6 °C and maximally 1.25 °C at an ambient temperature of 25 °C [39]. Any errors in measuring the cold junction temperature will directly appear as errors in the final measured temperature, therefore a calibration should be performed before using the thermocouples.

To calibrate the thermocouples, a water bath was heated with a precision cooker (Anova, A3.2-120V-US) over a range of 20 °C to 45 °C with 5 °C increments. At each of these set temperatures, the temperature was measured with the K-type thermocouple connected to the converter. A calibration curve was made in which the set temperature of the water bath measured by the Anova precision cooker was assumed to be the ground-truth temperature. To verify this, the temperature of the water bath was also measured with a thermometer (Thermapen 4, B17200071, United Kingdom) and a digital thermometer (Voltagecraft, model: #300) connected to another K-type thermocouple sensor (Control Company, VWR16.20-2005) which uses IEC584 temperature/voltage tables for conversion. The calibration curves are shown in Figure E.1. The verification thermometers both have a slope close to 1 and an intercept close to zero. This indicates a good agreement with the temperature measured by the Anova, and this confirms the suitability of the Anova thermometer as the reference temperature. The TC01 converter has a slope close to 1, but an intercept that significantly differs ($p<0.05$) from zero. This indicates the TC01 converter has a systematic offset compared to the reference temperature. In this case, the true temperature is 1.5 °C lower than indicated by the TC01 converter, therefore a correction needs to be applied using the equation of the linear fit in Figure E.1 (right graph).

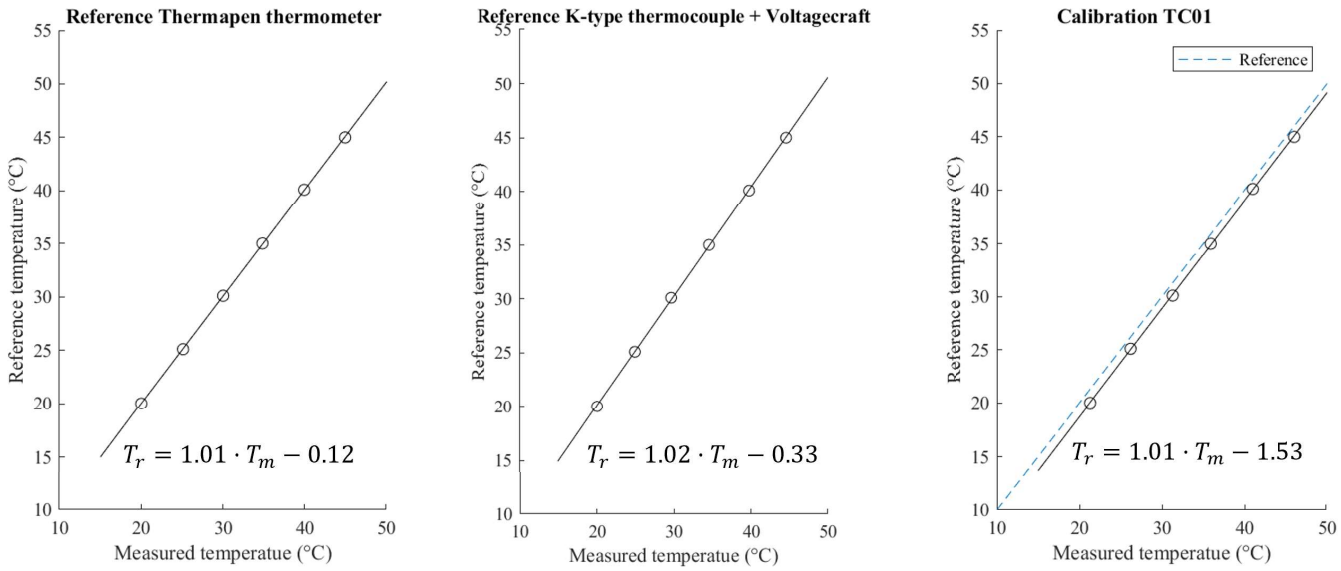

Figure E.1: Calibration curves of the thermocouples. The first and the second curve are reference measurements to validate the temperature measured by the Anova. The third curve is the calibration curve for a K-type thermocouple connected to a TC01-USB converter, which shows that the reference temperature (T_r) can be calculated by correcting the measured temperature (T_m) by -1.52 °C.

The magnitude of the error in the cold-junction compensation varies for each converter. It was also observed that the measured temperature offsets varied at different measurement moments with the same converter. Therefore, the thermocouples need to be calibrated before every measurement. This can be done by measuring the offset of the thermocouples compared to one ground-truth reference temperature, such as the 25 °water in the imaging bowl of the PAMMOTH. Calibration at only one temperature is sufficient, because the calibration curves (Figure E.1) showed a linear relation in the temperature range of 20-40 °C.

Additional results temperature homogeneity

F

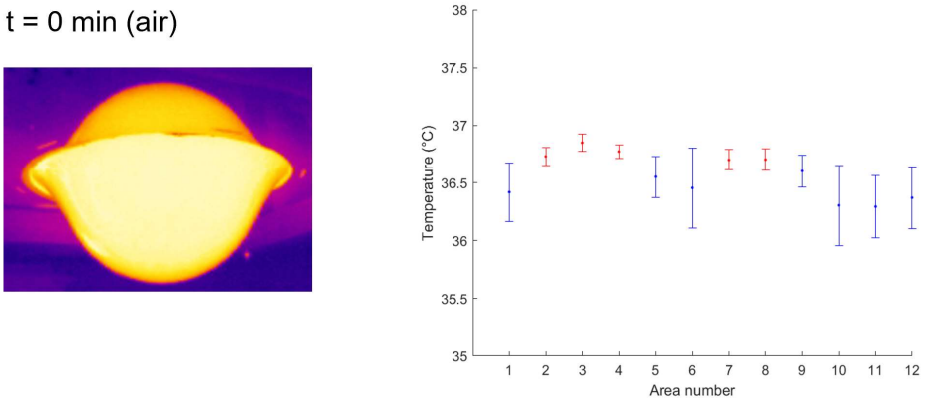

Figure F.1: Left: Snapshot of phantom with 37 °C water flow in experiment 1B after 0 minutes in a 25 °C water bath, and right: Mean and standard deviation of surface temperature in twelve sampling area (see Figure 6.11)

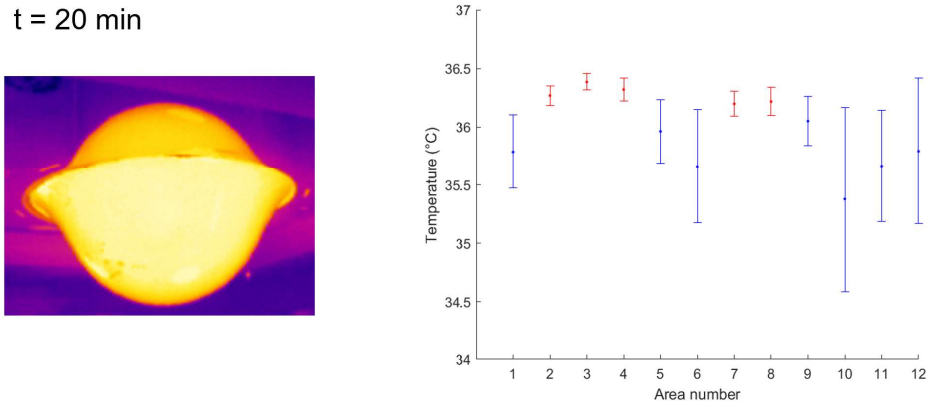

Figure F.2: Left: Snapshot of phantom with 37 °C water flow in experiment 1B after 20 minutes in a 25 °C water bath, and right: Mean and standard deviation of surface temperature in twelve sampling area (see Figure 6.11)

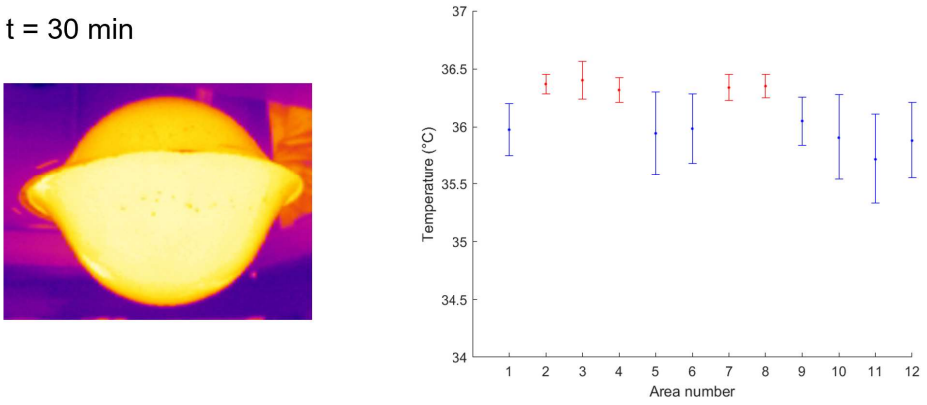

Figure F.3: Left: Snapshot of phantom with 37 °C water flow in experiment 1B after 30 minutes in a 25 °C water bath, and right: Mean and standard deviation of surface temperature in twelve sampling area (see Figure 6.11)

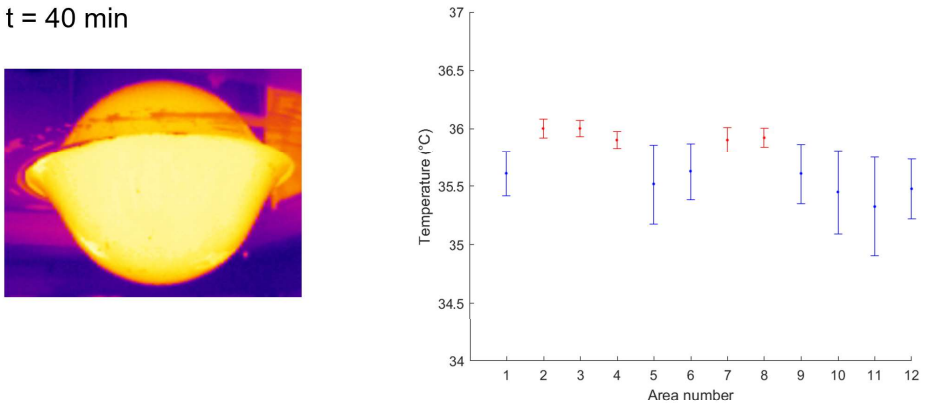

Figure F.4: Left: Snapshot of phantom with 37 °C water flow in experiment 1B after 40 minutes in a 25 °C water bath, and right: Mean and standard deviation of surface temperature in twelve sampling area (see Figure 6.11)

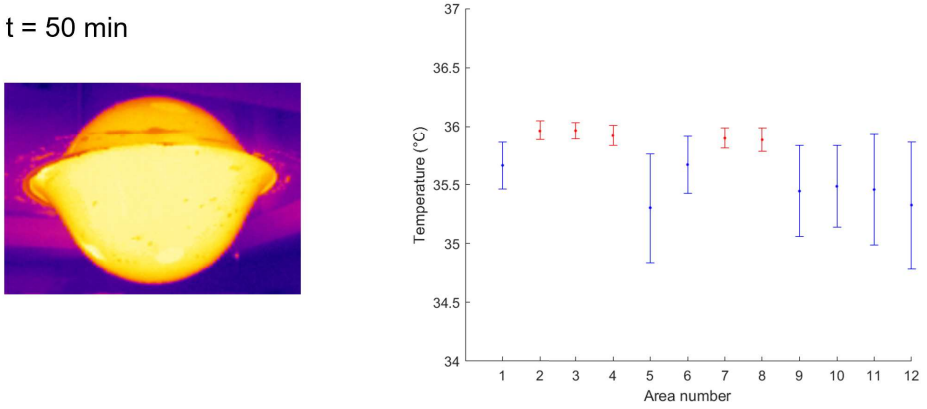

Figure F.5: Left: Snapshot of phantom with 37 °C water flow in experiment 1B after 50 minutes in a 25 °C water bath, and right: Mean and standard deviation of surface temperature in twelve sampling area (see Figure 6.11)

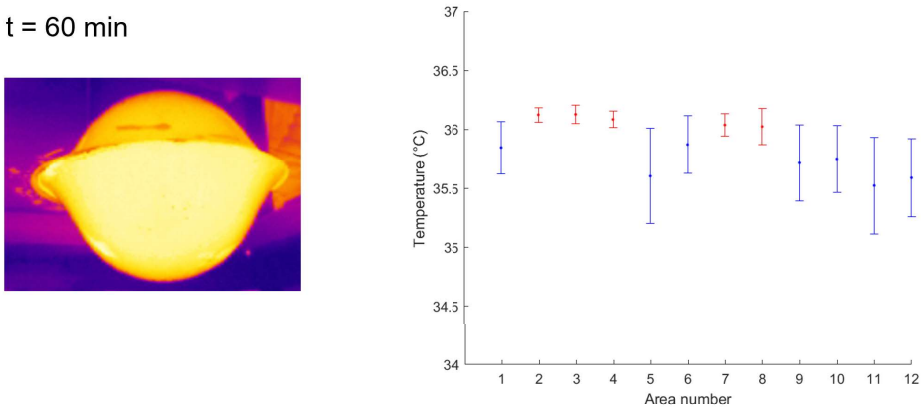

Figure F.6: Left: Snapshot of phantom with 37 °C water flow in experiment 1B after 60 minutes in a 25 °C water bath, and right: Mean and standard deviation of surface temperature in twelve sampling area (see Figure 6.11)

Additional results PA reconstructions

G

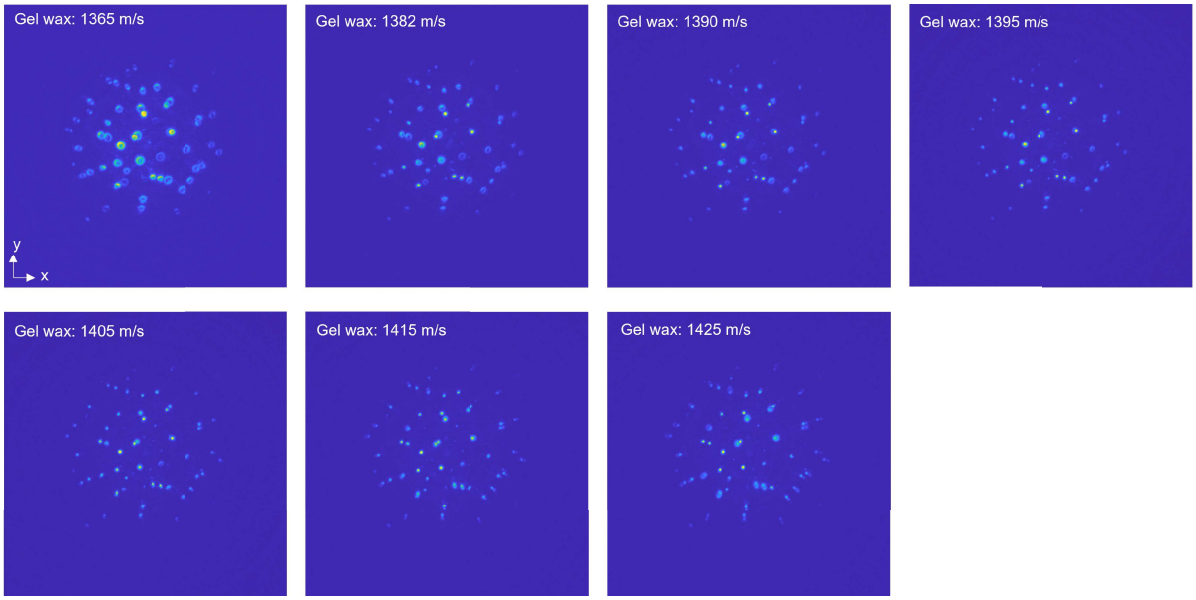

Figure G.1: MIPs of PA reconstructions (xy-plane) of measurement 5 (phantom water layer at 35 °C and gel wax at 40 °C), for different speed of sounds assigned to gel wax.

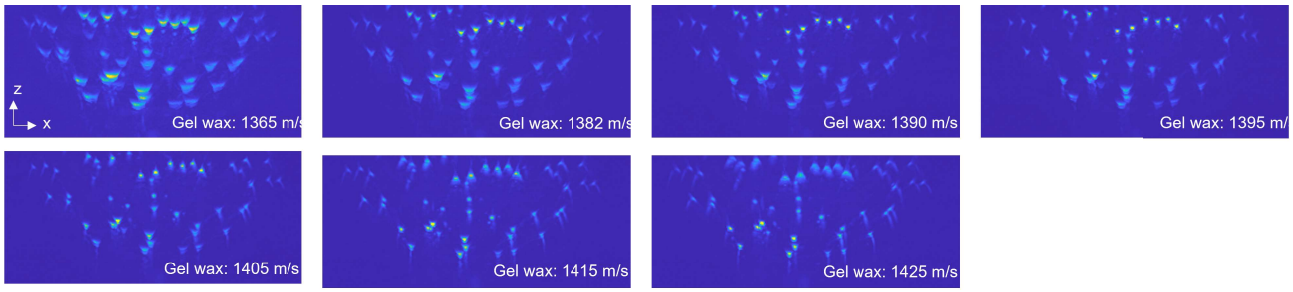

Figure G.2: MIPs of PA reconstructions (zx-plane) of measurement 5 (phantom water layer at 35 °C and gel wax at 40 °C), for different speed of sounds assigned to gel wax.